JAERI-Tech
98-059

PRELIMINARY THERMO-MECHANICAL ANALYSIS OF ITER BREEDING BLANKET

January 1999

Shigeto KIKUCHI, Toshimasa KURODA
and Mikio ENOEDA

日本原子力研究所
Japan Atomic Energy Research Institute

本レポートは，日本原子力研究所が不定期に公刊している研究報告書です。
入手の問合わせは，日本原子力研究所研究情報部研究情報課（〒319－1195 茨城県那珂郡東海村）あて，お申し越しください。なお，このほかに財団法人原子力弘済会資料センター（〒319－1195 茨城県那珂郡東海村日本原子力研究所内）で複写による実費頒布をおこなっております。

This report is issued irregularly.
Inquiries about availability of the reports should be addressed to Research Information Division, Department of Intellectual Resources, Japan Atomic Energy Research Institute, Tokai-mura, Naka-gun, Ibaraki-ken 〒319－1195, Japan.

編集兼発行　日本原子力研究所

Preliminary Thermo-mechanical Analysis of ITER Breeding Blanket

Shigeto KIKUCHI, Toshimasa KURODA and Mikio ENOEDA

Department of Fusion Engineering Research
Naka Fusion Research Establishment
Japan Atomic Energy Research Institute
Naka-machi, Naka-gun, Ibaraki-ken

(Received December 9 ,1998)

Thermo-mechanical analysis has been conducted on ITER breeding blanket taking into account thermo-mechanical characteristics peculiar to pebble beds. The features of the analysis are to adopt an elasto-plastic constitutive model for pebble beds and to take into account spatially varying thermal conductivity and heat transfer coefficient, especially in the Be pebble bed, depending on the stress.

ABAQUS code and COUPLED TEMPERATURE-DISPLACEMENT procedure of the code are selected so that thermal conductivity is automatically calculated in each calculation point depending on the stress. The modified DRUCKER-PRAGER/Cap plasticity model for granular materials of the code is selected so as to deal with such mechanical features of pebble bed as shear failure flow and hydrostatic plastic compression, and capability of the model is studied. The thermal property-stress correlation used in the analysis is obtained based on the experimental results at FZK and the results of additional thermo-mechanical analysis performed here. The thermo-mechanical analysis of an ITER breeding blanket module has been performed for four conditions : case A ; nominal case with spatial distribution of thermal conductivity and heat transfer coefficient in Be pebble bed depending on the stress, case B ; constant thermal conductivity, case C ; thermal conductivity = -20% of nominal case, and case D ; thermal conductivity = +20% of nominal case. In the nominal case the temperature of breending material (Li_2ZrO_3) ranges from 317℃ to 554℃ and the maximum temperature of Be pebble bed is 446℃. It is concluded that the temperature distribution is within the current design limits.

Though the analyses performed here are preliminary, the results exhibit well the qualitative features of the pebble bed mechanical behaviors observed in experiments.

For more detail quantitative estimates of the blanket performance, further investigation on mechanical properties of pebble beds by experiment, including pebble-wall friction and behaviors of pebbles subjected to tensile stresses and the improvement of the analysis model and the calculation code are required.

Keywords : ITER, Breeding Blanket, Pebble Bed, Drucker-Prager, Thermal Analysis, Stress Analysis

ITER増殖ブランケットの熱・応力解析

日本原子力研究所那珂研究所核融合工学部
菊池　茂人・黒田　敏公・榎枝　幹男

(1998年12月9日受理)

ペブル充填層に特有な熱・機械的特性を考慮してITER増殖ブランケットの熱・応力解析を実施した。本解析の特徴は、ペブル充填層に粉体（地盤）解析用の弾塑性モデルを採用したこと、及びペブル充填層の熱伝導率や容器壁近傍における熱伝達率が圧縮応力に依存して変化する特性を考慮したことである。

解析には、汎用の熱・構造解析コードであるABAQUSを使用し、熱伝導率、熱伝達率の圧縮応力依存性を考慮するため「Coupled Temperature－Displacement Procedure」を採用して熱・応力連成解析を実施した。弾塑性モデルとしては、地盤解析で使用される「Drucker－Prager／Cap plasticity」モデルを採用した。本モデルは、せん断による破壊面の他、静水圧による塑性圧縮を記述する降伏面を備えており、本モデルの妥当性についての検討も実施した。

ペブル充填層の熱伝導率及び熱伝達率と圧縮応力との関係については、FZKによる実験結果を基に評価した。また、同実験の再現計算を実施して本解析で使用した手法を検証した。

上述した解析手法により、空間的に一様な熱伝導率を基に設計されたITER増殖ブランケットを解析した。解析は、次の4ケースについて行った。

ケースA：基準ケース（熱伝導率及び熱伝達率の応力依存性を考慮）
ケースB：一定熱伝導率
ケースC：基準ケースの-20%の熱伝導率
ケースD：基準ケースの+20%の熱伝導率

基準ケースの増殖材（Li_2ZrO_3）の温度は、317℃から554℃の範囲にあり、Beの温度は約450℃以下であり、ペブル充填層の粉体としての熱・機械特性を考慮した解析によって、各材料の温度が目標とされている範囲を満たすことが分かった。

本解析は、予備的なものであり、今後、ペブル充填層のモデル化や熱特性の応力依存性に関し、ペブルと容器壁との摩擦や引張り応力時のペブル充填層の挙動等についても実測データに基づく詳細な検討を行い、増殖ブランケットの熱・応力解析手法の確立を図る必要がある。

那珂研究所：〒311-0193　茨城県那珂郡那珂町向山801-1

This is a blank page.

Contents

目　　次

1. Introduction

ITER (International Thermonuclear Experimental Reactor) is required to generate some amount of tritium basically comparable to its consumption in the Enhanced Performance Phase. Tritium production is accomplished by breeding blanket, which is composed of tritium breeding material and neutron multiplier. The breeding blanket of ITER [1,2] is designed to use currently Li_2ZrO_3 pebbles contained in the breeder rods as tritium breeding material and Be pebbles filled around the breeder rods in the basic cell as neutron multiplier as shown in Fig. 1.1. In the breeding blanket design, one of critical issues is caused by tight limitations on the breeder and Be temperatures for tritium recover from the breeder, materials integrity and safety aspect in case of accident. Therefore precise thermo-mechanical analysis is required. However, the analysis is very difficult because pebble bed shows such complex thermal and mechanical features as:

①Pebble bed effective thermal conductivity and near wall thermal conductance spatially vary depending on its compressive stresses.

②Pebble bed shows such characteristics of granular materials as shear failure flows caused by shear stress and plastic consolidations caused by hydrostatic compression [3].

③Thermal conductivity determining temperature distribution depends on compressive stress and in turn differential thermal expansion determining compressive stress depends on temperature distribution.

So far very simple analysis model has been studied such that pebble bed was modeled as a continuum with only elastic property. Therefore pebble bed effective elastic constant and Poisson's ratio were mainly measured concerning mechanical property of pebble bed, e.g. at UCLA [4]. As for the thermal property, effective thermal conductivity and near wall conductance of Be binary pebble bed was obtained in FZK as a function of $\Delta L/L$, which is a measure for representing compressive strain of pebble bed [5]. Based on this correlation, an effective thermal conductivity averaged over a specified region in the breeding blanket can be estimated.

The objective of present report is to investigate thermo-mechanical analysis methods and models so as to take into account those thermal and mechanical characteristics of pebble beds, and to evaluate preliminarily the performance of the ITER breeding blanket.

In Chapter 2 the mechanical analysis method used here and a trial analysis are described. In Chapter 3 the correlation between thermal property and

compressive stress of Be binary pebble bed is evaluated with the experimental results at FZK. The thermo-mechanical analysis procedure of breeding blanket (pebble bed) used here and a trial analysis on the experiment by this procedure are described in Chapter 4. Analysis of ITER breeding blanket is given in Chapter 5.

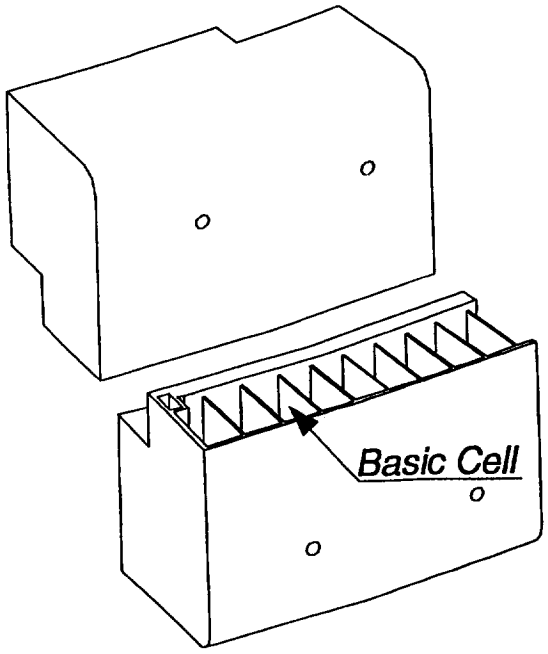

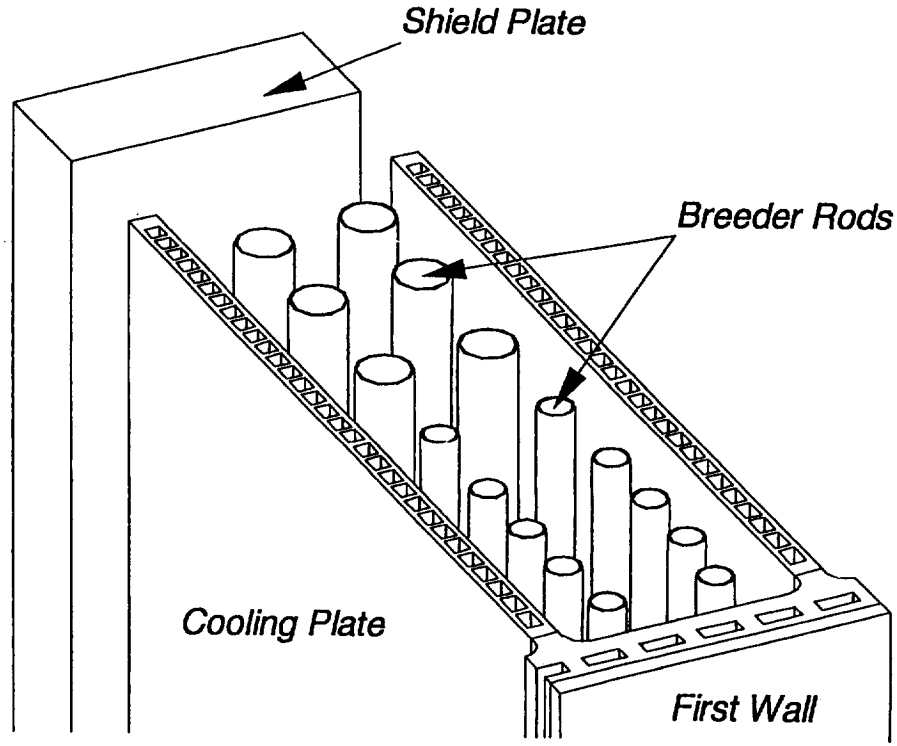

Detail of a basic cell (Be pebble bed removed for clarity)

Fig. 1.1 ITER Breeding Blanket [1]

2. Mechanical Analysis Method

2.1 Selection of Analysis Model

General purpose thermo-mechanical analysis codes such as NASTRAN and ABAQUS are able to analyze pebble beds, which are generally modeled as continuum of plastic property in the analysis. The modified DRUCKER-PRAGER/Cap plasticity model (cap model) of ABAQUS code is selected here because this model can treat hydrostatic plastic compression most properly as mentioned below. The constitutive equation of the cap model can handle the two yield surfaces expressing the features of pebble beds as shown in Fig. 2.1: 1) Shear failure surface providing shearing flow, 2) "Cap" bounding the yield surface in hydrostatic compression, thus providing an plastic hardening mechanism to represent plastic compaction. In the region bounded by the two yield surfaces, pebble beds show elastic behavior. If the stress condition changed to reach one of the surfaces, shear failure or plastic compaction occurs according to the surface. The cap position is generally enlarged by cap hardening effect when plastic compression occurs. Fig. 2.2 shows flow potential of this model, defining its plastic flow. Associated flow in the cap region and non-associated flow in the shear failure region are used in the model. Detailed explanation is given in the theory manual of ABAQUS code [6].

2.2 Trial Mechanical Analysis

Trial mechanical analysis using the cap model has been performed for the uniaxial compressive experiments conducted by UCLA [4]. In the experiments, an apparatus shown in Fig. 2.3 was used, axial compressive force was loaded to single size pebble beds of Al and Li_2ZrO_3, and the correlation between the axial compressive stress and the axial compressive strain was obtained as shown in Figs. 2.4 and 2.5. In Fig. 2.4 the axial compressive strain remaining after the 1st unloading process represents hydrostatic plastic compaction which is not observed in case of metal. The hysterisis behavior is observed in the stress - strain plane as shown in Figs. 2.4 and 2.5.

2.2.1 Analysis Condition

1) Analysis case

The uniaxial compressive experiment with Al single size pebble bed conducted by UCLA

2) Analysis model

2D cylindrical analysis model shown in Fig. 2.6. (Only the pebble bed is modeled, thus the friction between the pebbles and the container wall is assumed perfectly smooth.)

3) Analysis step

Step1 : 1st loading ; u=0.635mm (ε_a=0.01)
Step2 : 1st unloading
Step3 : 2nd loading ; u=1.27mm (ε_a=0.02)

In the loading steps, axial displacements (u) are loaded so that the expected axial strains (ε_a) are obtained. In the unloading step, the axial displacement loads was fully removed.

4) Analysis code / option

ABAQUS5.7 / modified DRUCKER-PRAGER/Cap plasticity model

5) Mechanical data

Mechanical data used for the cap model analysis are listed in Table 2.1. The elastic constant and cap hardening data are approximately estimated with the UCLA experimental data except for shear failure data as follows.

a) Elastic constant and cap hardening data

Young's modulus and cap hardening data are obtained by the assumption that, in Fig. 2.4, the 1st loading step represents cap hardening process and the 1st unloading step represents elastic process as redrawn in Fig. 2.7

Young's modulus

Young's modulus is calculated as described below:

$$E = \frac{1}{(\varepsilon_{a1} - \varepsilon_{a2})}(\sigma_{a1} - 2\nu\sigma_r) = (1 - 2\nu k_0)\frac{\sigma_{a1}}{(\varepsilon_{a1} - \varepsilon_{a2})} = 2.4GPa \quad \text{--------- (2.1)}$$

E : Young's modulus
ε_{a1}, ε_{a2} : axial strain (0.0377, 0.0296 ; fixed with Fig. 2.7)
σ_{a1} : axial stress (23.5MPa ; fixed with Fig. 2.7)
ν : Poisson's ratio (0.25 ; by UCLA [4])
k_0 : $=\sigma_r/\sigma_a$ (0.339 ; by UCLA [4])

Poisson's ratio

The Poisson's ratio evaluated by UCLA [4] is used.

$\nu = 0.25$

b) Cap hardening data

Cap position is determined by a set of hydrostatic pressure and plastic volume strain in the process of a hydrostatic plastic compression. For the cap position of point A in Fig. 2.7,

$$p = \frac{1}{3}(\sigma_{a1} + 2\sigma_r) = \frac{1}{3}(1 + 2k_0)\sigma_{a1} = 13.2MPa \qquad \text{---------- (2.2)}$$

$$\varepsilon_{vol}^{Pl} = \varepsilon_{a2} = 0.0296$$

(Volume strain (ε_{vol}) equals to axial strain (ε_a) in a uni-axial case . The plastic strain of point A is assumed to be the remaining strain after unloading (ε_{a2} at point B).) The minimum cap position also has to be given, which is defined as the pressure at which hydrostatic plastic compression begins. It seems very low and can not be clearly seen from Fig. 2.4. However since very low cap hardening pressure makes convergence of the analysis deadly worse, the minimum cap position of 1 MPa (at $\varepsilon_{vol}^{Pl} = 0$) is assumed here. The inclination of Cap hardening line defined as cap hardening pressure divided by plastic volume strain is 440 MPa (=13.2/0.0296) and is nearly 1/5 of Young's modulus (2.4 GPa).

c) Shear failure data

Among the data related to shear failure summarized in Table 2.1, friction angle and cohesion are especially important.

Friction angle

It is assumed that the friction angle of Mohr-Coulomb model is 20° in the case of Be and Li_2ZrO_3 binary pebble beds. Then, the friction angle of DRUCKER-PRAGER/Cap model is determined according to the analysis model or type of elements as follows [6]:

- 2-D cylindrical model:

$$\tan\beta = \frac{6\sin\phi}{3 - \sin\phi} \qquad \text{---------- (2.3)}$$

ϕ : friction angle of Mohr-Coulomb (20° : assumed at present)

β : friction angle of DRUCKER-PRAGER/Cap model
= 37.6° (calculated with above equation)

- 2-D X-Y model with plane strain condition:
$\beta = 30.6°$ (for ϕ=20° [6])

Cohesion

The cohesion is temporarily set to be 1/2 of the minimum cap pressure for Be pebble

bed because of the convergence in computation.

2.2.2 Result of analysis

Analysis results for the uni-axial compressive experiment are shown in Figs. 2.8 - 2.12. The mechanical behavior of the pebble bed is divided into the following six processes as shown in these figures.

(1) Elastic compression (1^{st} loading)
(2) Hydrostatic plastic compression (1^{st} loading)
(3) Elastic expansion (1^{st} unloading)
(4) Shear failure (1^{st} unloading)
(5) Elastic compression (2^{nd} loading)
(6) Hydrostatic plastic compression (2^{nd} loading)

The features of each process are described below.

(1) Elastic compression (1^{st} loading)
The axial compressive stress increases according to the Young's modulus (Fig. 2.8 and Fig. 2.10) to reach the minimum cap surface (Fig. 2.9).

(2) Hydrostatic plastic compression (1^{st} loading)
The inclination of hydrostatic plastic compressive process is lower than that of the elastic compressive process (Fig. 2.8). The axial plastic strain as well as the radial plastic strain is caused by the hydrostatic compression (Fig. 2.11).

(3) Elastic expansion (1^{st} unloading)
The axial compressive stress decreases according to the Young's modulus (Fig. 2.8) and becomes smaller than the radial stress in the unloading process (Fig. 2.12). The latter behavior is observed in the UCLA experiment [4]. The shear stress reaches the shear failure surface (Fig. 2.9). The dotted line in Fig. 2.9 is drawn in order to show a presumed pass to supplement the lack of analysis points.

(4) Shear failure flow (1^{st} unloading)
The shear failure flow occurs (Fig. 2.9). The shear failure flow causes the hystrerisis behavior in the strain-stress plane as shown in Fig. 2.8. The hysiterisis behavior is seen in the experimental result at UCLA (Fig. 2.4 and 2.5).

(5) Elastic compression (2^{nd} loading)

The elastic range is enlarged by the cap hardening effect that is caused by the 1st loading process.

(6) Hydrostatic plastic compression (2nd loading)
The same behavior as the 1st loading is observed.

Consequently the results using the cap model qualitatively represent well the pebble bed mechanical behavior observed in the experiment, i.e. hydrostatic plastic compression and hysteresis stress-strain curve due to shear failure. It can be concluded from this trial analysis that the cap model is one of the promising methods to be used for the analysis of the breeding blanket. It should be noted that since the mechanical behavior of the pebble bed is ruled by the inclination of cap hardening line after the minimum cap position is reached, inclination of cap hardening line and minimum cap position are very important on understanding and analyzing the pebble bed behavior as well as effective Young's modulus and Poisson's ratio.

Table 2.1 Mechanical data for analysis of uni-axial compressive experiment

a) Elastic constant

Young's modulus, E	2.4 GPa
Poisson's ratio, ν	0.25

b) Shear failure data

cohesion, d	0.5 MPa
friction angle, β	37.6°
parameter for cap center shift, R	0.5*
initial plastic volume strain, $\varepsilon_{vol}^{Pl}(0)$	0. **
parameter for transition surface, α	0. *
yield stress ratio (tension/compression), K	1. *

c) Cap hardening data

No.	p(MPa)	ε_{vol}^{Pl}	Comment
1	1.	0.	minimum cap position
2	13.2	0.0296	Point A in Fig. 2.7

*: Typical values are temporarily assumed based on ABAQUS/Standard user's manual [6].

**: No initial plastic volume strain is assumed.

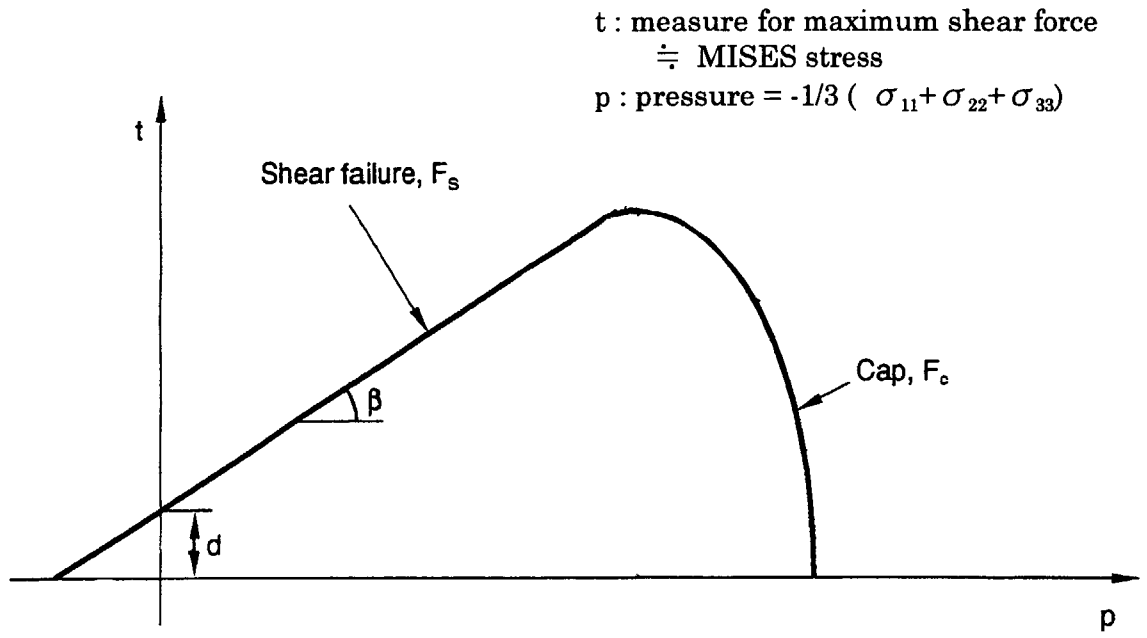

Fig. 2.1 Modified Drucker-Prager/Cap model: yield surfaces in the p-t plane [6]

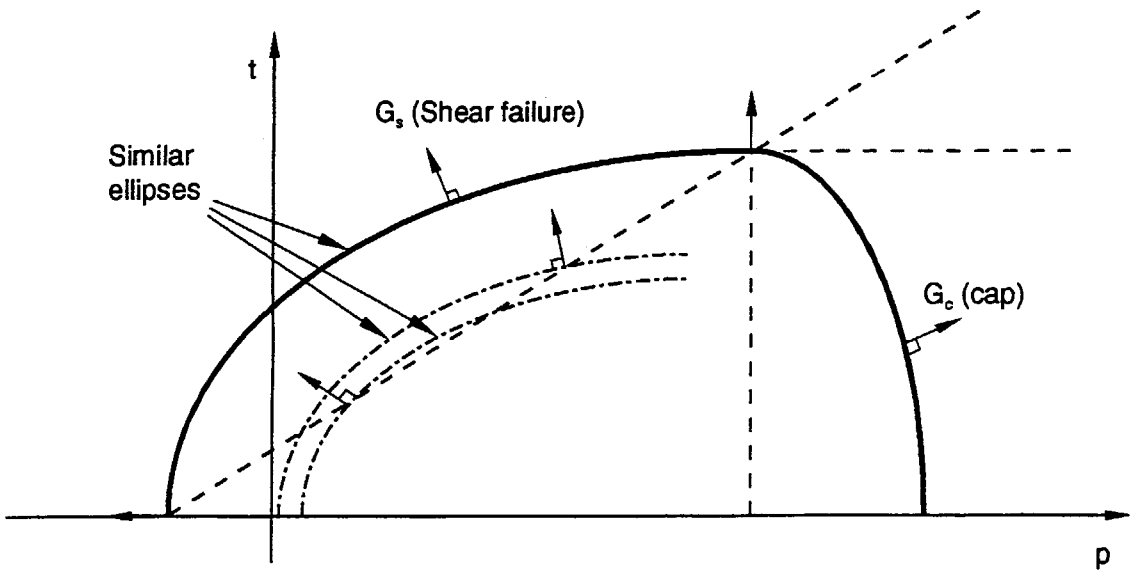

Fig. 2.2 Modified Drucker-Prager/Cap model: flow potential in the p-t plane [6]

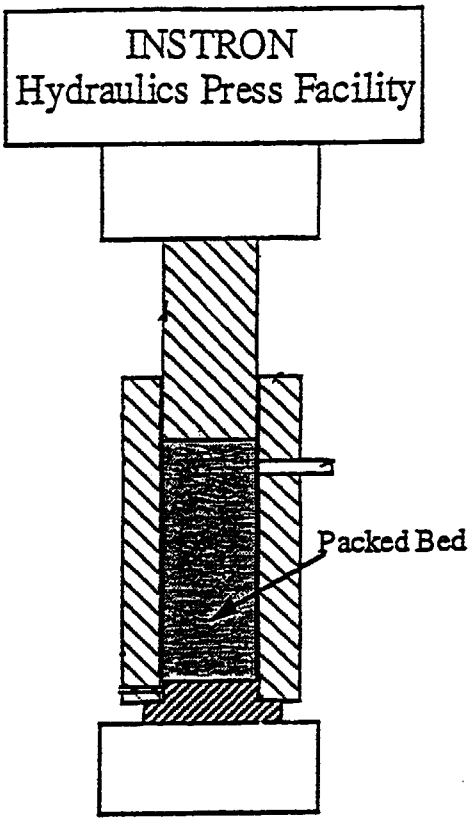

Fig. 2.3 Uniaxial compression test apparatus (UCLA [4])

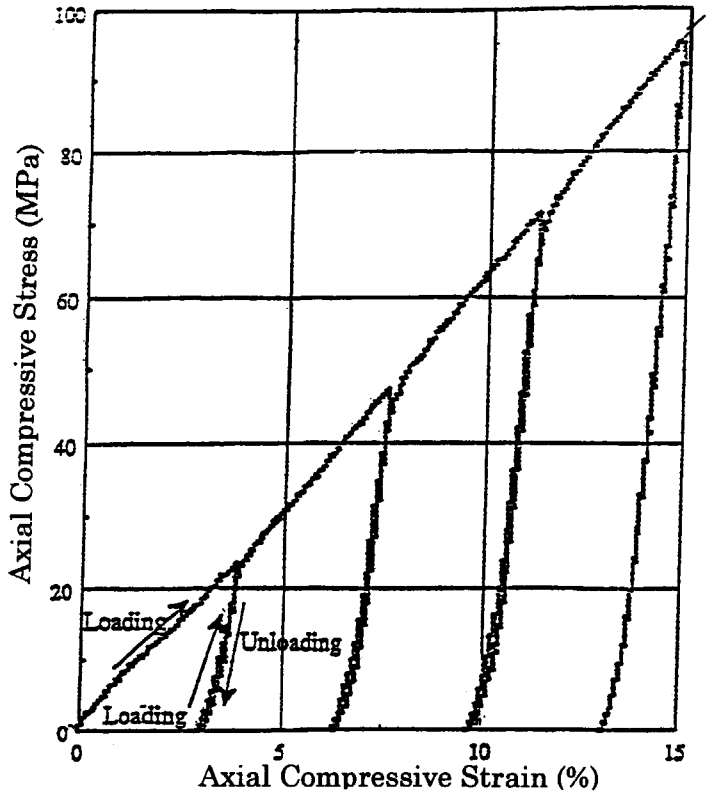

Fig. 2.4 Stress vs. Strain During Cyclic Loading and Unloading Tests (UCLA [4])
(Aluminum Packed Bed)

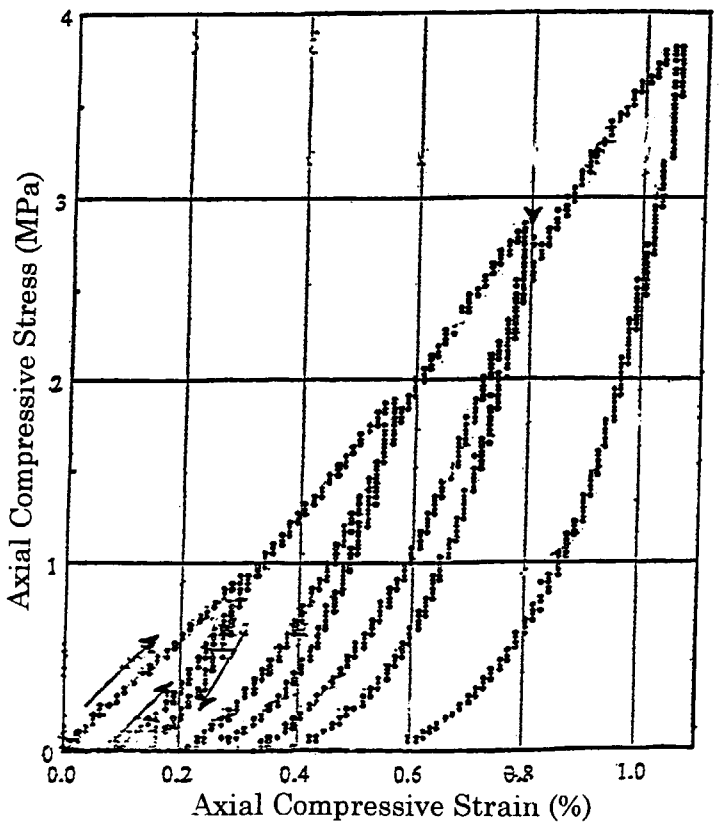

Fig. 2.5 Stress vs. Strain During Cyclic Loading and Unloading Tests (UCLA [4])
(Li2ZrO3 Packed Bed)

(2D cylindrical)

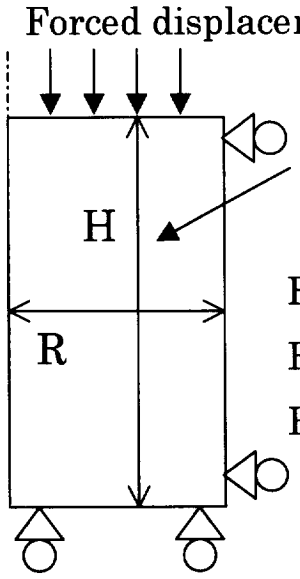

H: 63.5 mm*

R: 12.7 mm*

Boundary condition: no friction

Analysis Step

Step 1: 1st loading u=0.635mm(ε_a=0.01)

Step 2: 1st unloading

Step 3: 2nd loading u=1.27mm(ε_a=0.02)

(* assumed based on the figure in ref.[7])

Fig. 2.6 Analysis model of uniaxial compression test

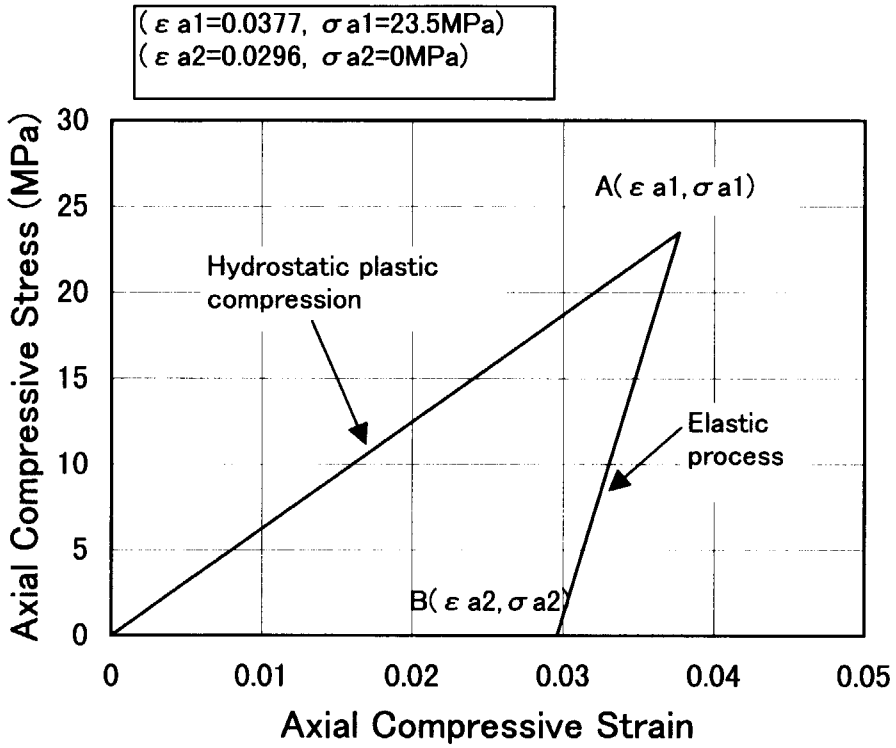

Fig. 2.7 Relation between the axial compressive strain and the axial compressive stress for Al single size bed (1st loading and 1st unloading in Fig. 2.4)

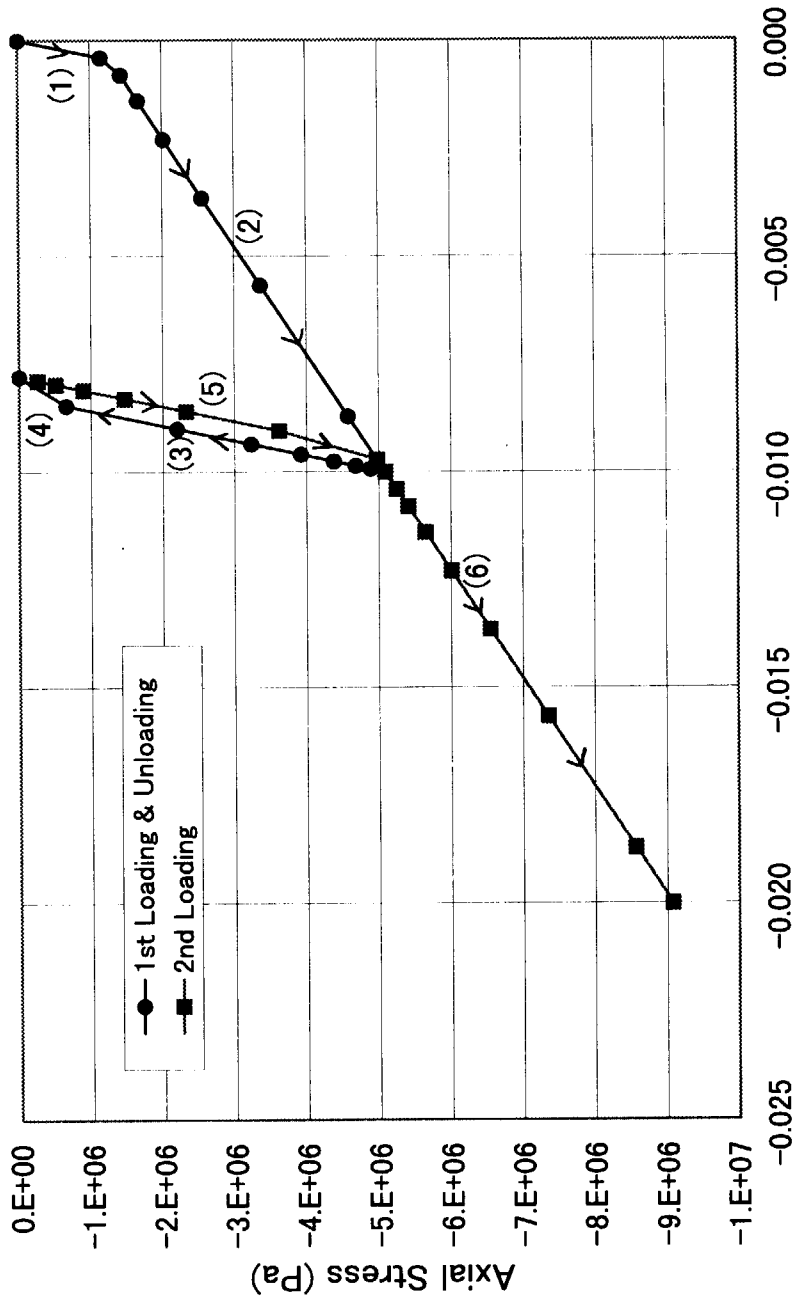

Fig. 2.8 Analyzed results of the uni-axial compressive experiment (Axial stress vs. axial strain)

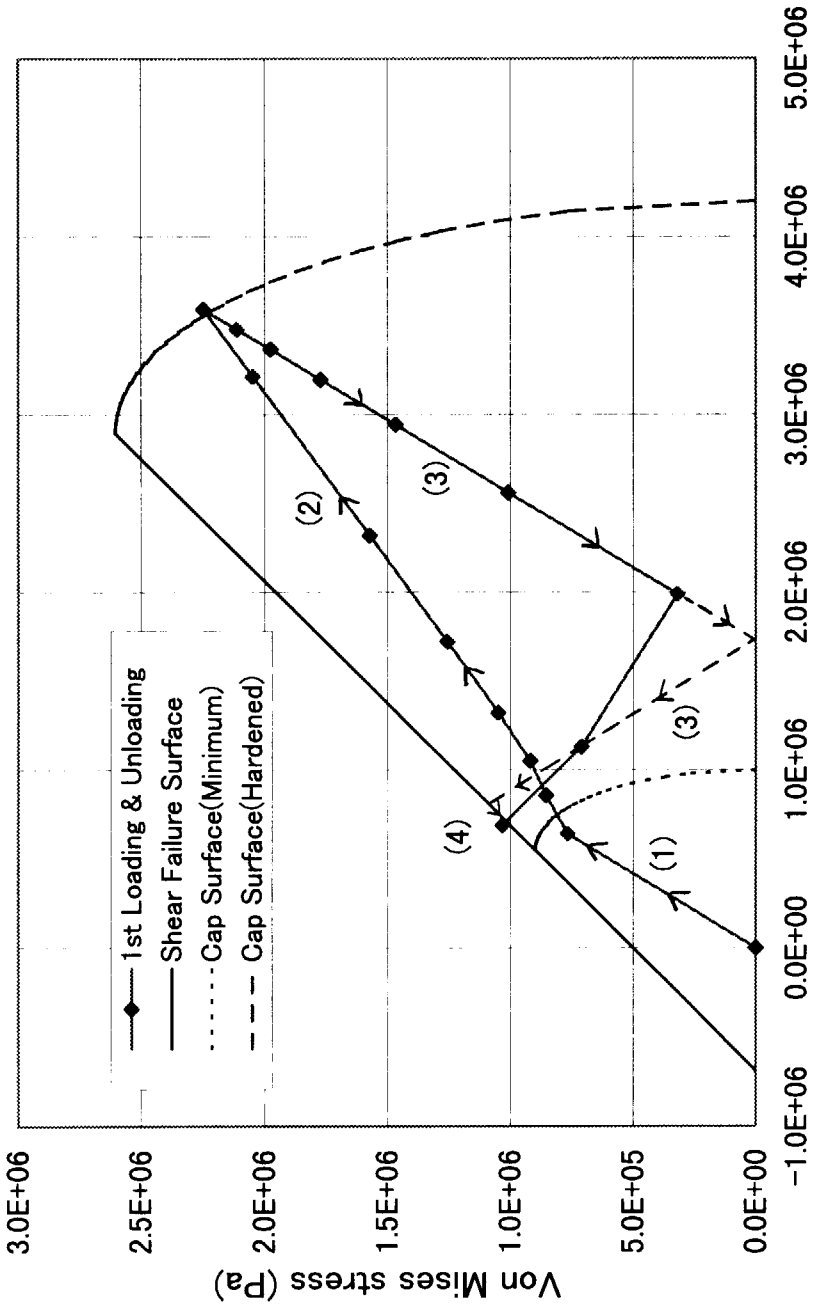

Fi. 2.9 Analyzed results of the uni-axial compressive experiment (Von Mises stress vs. hydrostatic pressure)

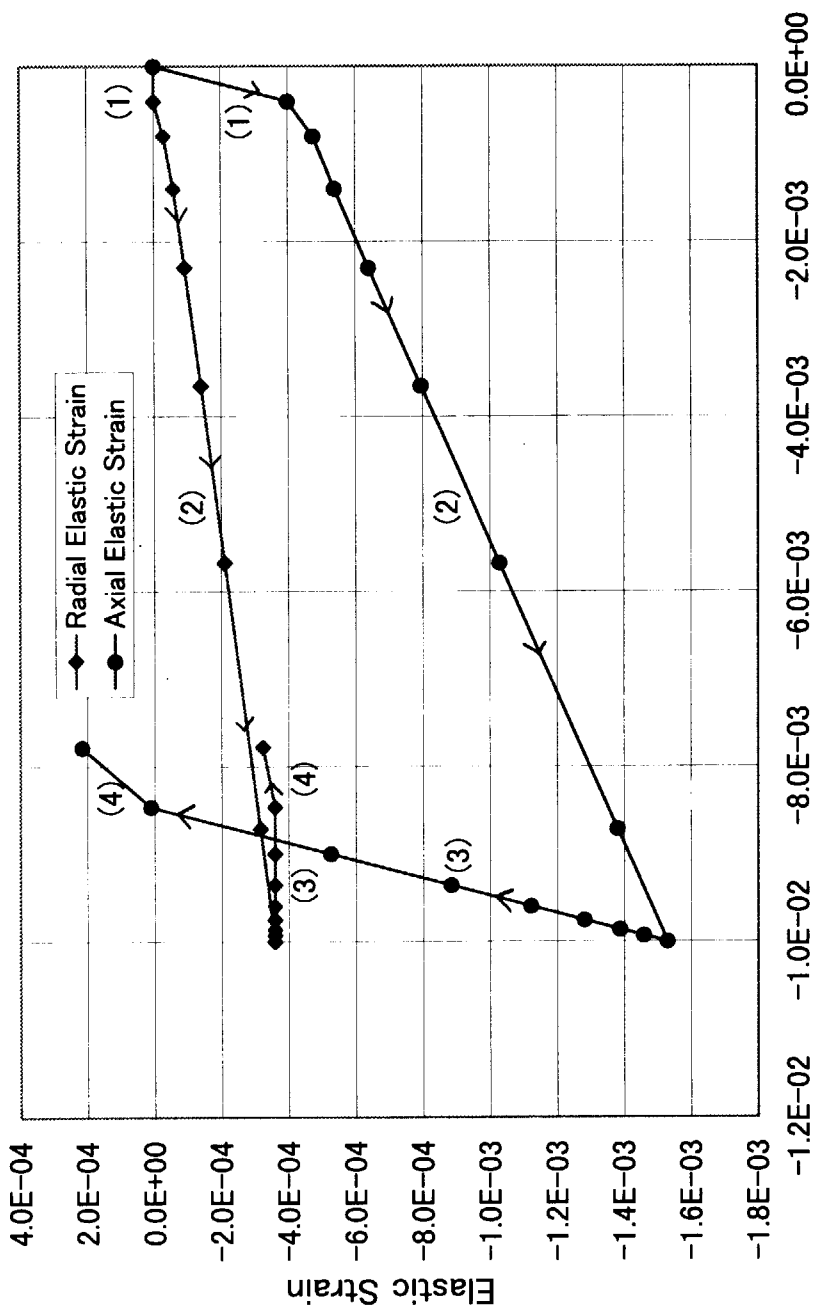

Fig. 2.10 Analyzed results of the uni-axial compressive experiment (Elastic strain vs. total axial strain)

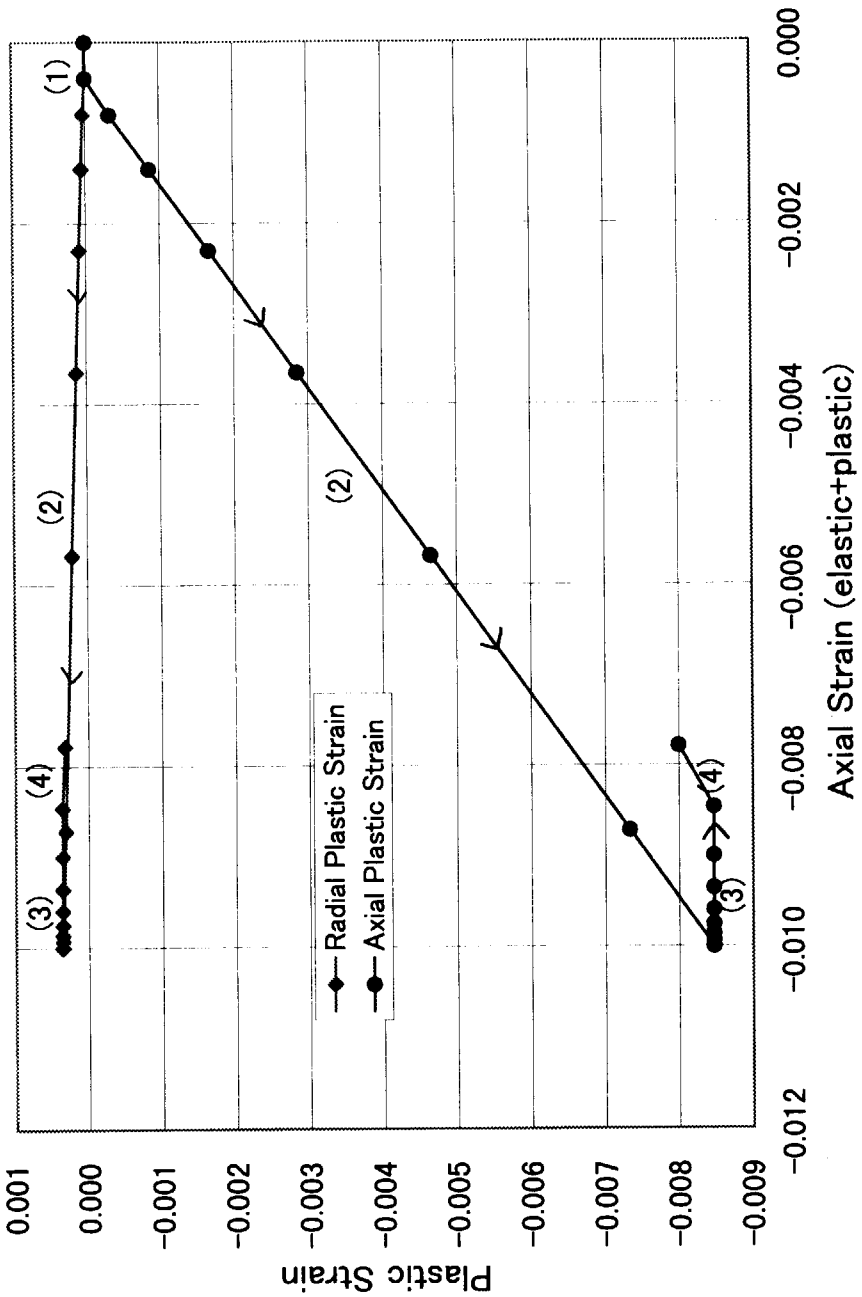

Fig. 2.11 Analyzed results of the uni-axial compressive experiment (Plastic strain vs. total axial strain)

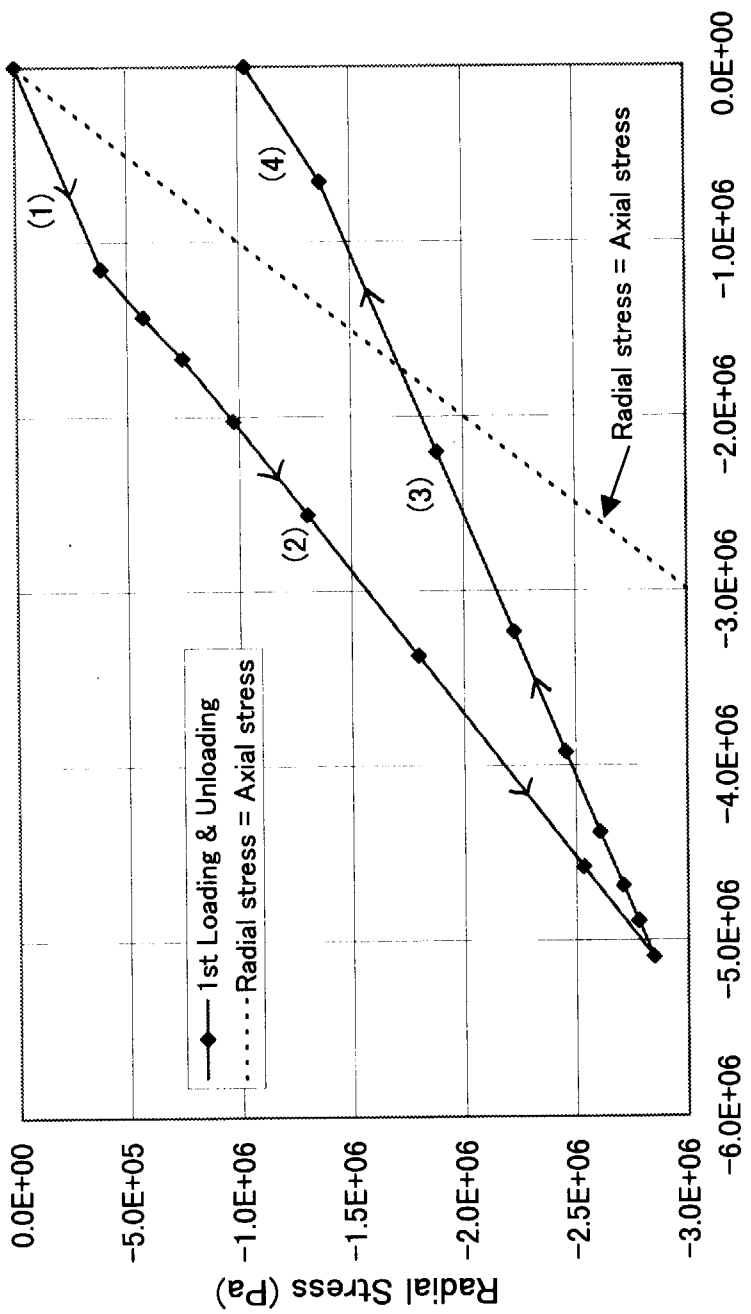

Fig. 2.12 Analyzed results of the uni-axial compressive experiment (Radial stress vs. axial stress)

3. Thermal Property-Stress Correlation

It was reported that effective thermal conductivity and wall heat transfer coefficients of pebble beds increased by compressive stress/force of the pebble bed [5]. Correlation between those thermal properties and compressive stress are derived for Be binary pebble bed here through analysis of the stress distribution in the pebble bed of the heat transfer experiment performed by FZK [5]. Then, the obtained correlation on the thermal conductivity is compared to the experimental data measured for Al single sized pebble bed by UCLA [7].

3.1 FZK Experiment [5]

Effective thermal conductivity of Be binary pebble bed was measured from the temperature gradient across a pebble bed contained in an annular cylinder. Typical experimental result of temperature profile is shown in Fig. 3.1. The radial compressive stress was generated in the annular cylinder by a differential thermal expansion among the inner and outer tubes and the pebble bed. Then the measured thermal property was correlated to the compressive strain of pebble bed defined as $\Delta L/L$ by FZK. The relation for Be binary pebble bed is reported as follows:

Packed pebbles : Be binary pebble (2mm ϕ (64.5%)+0.2mm ϕ (16.3%);
total packing factor 80.8%)

$$\lambda[W/mK] = \left(7.3145 + 1.00652\times10^{-4}T_m\right)\left(1 + 7.259\frac{\Delta L}{L}[\%]\right) \quad \text{---------- (3.1)}$$

$$h[W/cm^2K] = 6.138\times10^{-2} \bullet f \bullet e^{0.00353327Tw} \quad \text{---------- (3.2)}$$

with $f = 4.023 + 54.63\frac{\Delta L}{L}$ for $\frac{\Delta L}{L}[\%] \geq 0.015$

and $f = 1$ for $\frac{\Delta L}{L}[\%] < 0.015$

Tm or Tw 130-600°C

$\Delta L/L$ 0-0.1%

λ = effective thermal conductivity of the bed [W/mK]
L = thickness of the bed in the direction of the heat flow (=R2-R1 [cm])
R1 = outer radius of the inner heating tube [cm]
R2 = inner radius of the outer containing tube [cm]
T = Tm = average temperature of the bed [°C]
Tw = temperature of the outer surface of the inner tube

h = heat transfer coefficient between bed and containing walls at the outer surface of the inner tube [W/cm^2 ℃]

α_{Be} = thermal expansion coefficient of beryllium at Tm [K^{-1}]

α_{St} = thermal expansion coefficient of the containing walls of stainless steel [K^{-1}]

$\Delta L/L$ = percent difference between the thermal expansion of the bed and the confinement walls referred to the thickness of the bed

$$= 100 \times \left[\alpha_{Be}(T_m - T_0) + \frac{\alpha_{St2}R_2 - \alpha_{St1}R_1}{R_2 - R_1} T_0 - \frac{\alpha_{St2}R_2T_{w2} - \alpha_{St1}R_1T_{w1}}{R_2 - R_1} \right] \quad \text{---- (3.3)}$$

3.2 Analysis of the Heat Transfer Experiment

Stress distribution of the heat transfer experiment system of FZK is analyzed so that the measured thermal property is correlated to its compressive stress.

3.2.1 Analysis Condition

1) Analysis case

The heat transfer experiment with water cooling on the outside surface for subjecting compressive stresses to the pebble bed. Two cases were analyzed in terms of minimum cap position (see 5), b)).

2) Analysis model

- 2D cylindrical model shown in Fig. 3.2.

3) Analysis code / model

- ABAQUS 5.7
- modified DRUCKER-PRAGER/Cap plasticity model

4) Thermal properties

The effective thermal conductivity (λ) and heat transfer coefficient (h) of Be binary pebble bed are referred from the data experimentally evaluated by FZK [5]. The heat transfer coefficients are taken into account by incorporating a modified thermal conductivity for near wall element as described below.

$$\frac{1}{\lambda_M} = \frac{1}{\Delta x \times h} + \frac{1}{\lambda} \quad \text{---------- (3.4)}$$

λ_M : modified λ for element to take into account heat transfer coefficient

λ,h : effective thermal conductivity and heat transfer coefficient of Be binary pebble bed
Δx: width of near wall element (Fig. 3.2)

Thermal properties used here are as follows:

- λ for pebble bed bulk region : 12.07 W/mK
- λ_M for near wall element:
  a) at inner tube wall : 3.38 W/mK
  (element width=0.5mm; λ=12.07W/mK; h=0.94 W/cm^{2}K)
  b) at outer tube wall : 0.32 W/mK
  (element width:0.5mm; λ=12.07W/mK; h=0.066 W/cm^{2}K
  Since the h for the outer tube wall has not been measured by FZK, the h is evaluated with the correlation (Eq. (3.2)) using the condition T=20℃ and ΔL/L=0.)
- Thermal expansion coefficient of the pebble bed : the same values as base solid materials

5) Mechanical properties

Mechanical properties for the cap model analysis are summarized in Table 3.1.

a) Young's modulus

Since no experimental data is available for binary pebble beds at present, Young's modulus for Be single size pebble bed is temporarily assumed. The Young's modulus is estimated as 1.45 GPa by the analytic model of K.Walton [8] for uniaxial compression of perfectly smooth spheres as shown in Table 3.2 (Appendix A).

b) Cap hardening data

Cap hardening data are composed of a minimum cap position and at least one cap hardening pressure corresponding to a plastic volume strain. The minimum cap position is parametrically assumed (1 MPa and 0.1 MPa). The other cap hardening pressure is determined as shown in Table 3.1 based on the inclination of cap hardening line calculated as 1/5 of Young's modulus by the assumption that the inclination for Be binary pebble bed is similar to that for Al single size pebble bed. Namely,

$$p = \frac{E}{5} \times \varepsilon_{vol}^{Pl} = \frac{1450MPa}{5} \times 0.1 = 29MPa \qquad \text{---------- (3.5)}$$

ε_{vol}^{Pl} is assumed to be 0.1 which is never reached in the analysis.

c) Shear failure data

The shear failure data are the same as those used in section 2.2.1 except for the

cohesion data which are assumed to be half of minimum cap position (0.5 MPa, 0.05. MPa) as described in section 2.2.1.

3.2.2 Results of Analysis

Analyzed temperature distribution with uniform effective thermal conductivity independent on the stress is shown in Fig. 3.3. Large temperature gap at the outer wall does not agree with the measured temperature profile shown in Fig. 3.1. Later in Chapter 4, it will be shown that this discrepancy is removed with the model taking into account thermal conductivity and heat transfer coefficient depending on compressive stress.

Analyzed stress distributions in the pebble bed region are shown in Fig. 3.4 and Fig. 3.5 for minimum cap positions of 1 MPa and 0.1 MPa, respectively. In both figures, the maximum radial compressive stress in the inner region is about 2.5 times higher than the minimum one in the outer region. Therefore it is found that the difference of the minimum cap position causes only small change in the shape of radial stress profile. On the other hand, rather large difference in absolute values of the radial stresses is given by the difference. For example, the maximum compressive stress near the inner tube in the former case (Fig.3.4) is nearly 2.5 MPa while it is about 1.0 MPa in the latter case (Fig.3.5).

3.3 Thermal Property Correlation

FZK has experimentally evaluated the relation between $\Delta L/L$ and the thermal properties as described above. The $\Delta L/L$ is related to compressive stress here with the analyzed stress distribution of the experiment system.

1) Effective thermal conductivity

It could be assumed that the $\Delta L/L$ is in proportion to the radial averaged compressive stress in the experimental system because the $\Delta L/L$ is a sort of compressive strain defined as the difference between contraction of the container due to differential thermal expansion of inner and outer tubes and thermal expansion of pebble bed. The local effective thermal conductivity ($\lambda(r)$) of the experimental system could be also expressed as a 1st order function of a radial compressive stress ($\sigma_r(r)$) (Eq. (3.6)) because the average effective thermal conductivity (λ_{avg}) is expressed as a 1st order function of $\Delta L/L$ (Eq. (3.7) derived from Eq. (3.1)).

$$\lambda(r) = \lambda_0' + A' \times \sigma_r(r) \qquad \text{---------- (3.6)}$$

$$\lambda_{avg} = \lambda_0 + A \times \frac{\Delta L}{L} \qquad \text{---------- (3.7)}$$

λ_0, λ_0' : thermal conductivity without stress

A, A' : constants

The average thermal conductivity of the experiment system is obtained by integration of Eq. (3.6) with the σ(r) and weighting function w(r) of the system.

$$\lambda_{avg} = \frac{\int (\lambda_0' + A' \times \sigma_r(r)) w(r) dr}{\int w(r) dr} = \lambda_0' + A' \times \sigma_{r-avg} \qquad \text{---------- (3.8)}$$

By comparing Eq. (3.8) and Eq. (3.7), the next correlations are obtained because Eq. (3.8) and Eq. (3.7) must coincide in any experimental condition.

$$\lambda_0' = \lambda_0 \qquad \text{---------- (3.9)}$$

$$A' = \frac{A \times \left(\frac{\Delta L}{L}\right)_{avg}}{\sigma_{r-avg}} \qquad \text{---------- (3.10)}$$

By substituting Eq. (3.9) and Eq. (3.10) into Eq. (3.6),

$$\lambda(r) = \lambda_0 + \frac{A \times \left(\frac{\Delta L}{L}\right)_{avg}}{\sigma_{r-avg}} \times \sigma(r) = \lambda_0 + A \times \left(\frac{\left(\frac{\Delta L}{L}\right)_{avg}}{\sigma_{r-avg}} \sigma(r) \right) \qquad \text{-------- (3.11)}$$

Comparison of Eq. (3.11) and Eq. (3.7) shows that local effective thermal conductivity can be obtained by Eq. (3.1) with local ΔL/L defined by the next equation.

$$\frac{\Delta L}{L}(r) = \frac{\left(\frac{\Delta L}{L}\right)_{avg}}{\sigma_{r-avg}} \sigma(r) \qquad \text{---------- (3.12)}$$

Selection of the weighting function and range of integration in Eq. (3.8) fully depends on how the effective thermal conductivity is determined with the measured

temperature distributions. In this preliminary analysis, most general weighting function (w(r)=r) is selected for simple volumetric average.

$$(\sigma_{r-ave}) = \frac{\int \sigma_r(r) r dr}{\int r dr} \qquad \text{---------- (3.13)}$$

Calculated results are:

○Case for minimum cap position = 1MPa

$$\frac{\Delta L}{L}(\sigma) = \frac{0.0927}{1.37} \times \sigma \qquad \text{---------- (3.14)}$$

($\sigma \leqq$ 2.45 MPa (maximum stress in the analysis))

○Case for minimum cap position = 0.1MPa

$$\frac{\Delta L}{L}(\sigma) = \frac{0.0927}{0.54} \times \sigma \qquad \text{---------- (3.15)}$$

($\sigma \leqq$ 0.969 MPa (maximum stress in the analysis))

Using the above equations and Eq. (3.1), the correlation between the effective thermal conductivity and compressive stress is obtained.

○Case for minimum cap position = 1MPa

$$\lambda[W/mK] = \left(7.3145 + 1.00652 \times 10^{-4} T_m\right)\left(1 + 0.491 \times \sigma[MPa]\right) \qquad \text{---------- (3.16)}$$

($\sigma \leqq$ 2.45 MPa)

○Case for minimum cap position = 0.1MPa

$$\lambda[W/mK] = \left(7.3145 + 1.00652 \times 10^{-4} T_m\right)\left(1 + 1.25 \times \sigma[MPa]\right) \qquad \text{---------- (3.17)}$$

($\sigma \leqq$ 0.969 MPa)

With the above equations effective thermal conductivity is calculated as shown in Fig. 3.6. Though these relation is strongly affected by the data used for the stress analysis (a minimum cap position), the calculated thermal conductivity has small difference through employment of the consistent analytic data, as described in the later Chapter 4 (Fig. 4.3). For with a bigger minimum cap position, rate of increase in thermal conductivity by compressive stress get lower as shown in Fig. 3.6. With the same minimum cap position, compressive stress is calculated to be higher. Then the lower increase rate in thermal conductivity and higher compress stress is expected to cancel out in calculation of thermal conductivity.

The same correlation is measured for Al single pebble bed at UCLA [7]. For reference the above correlation for Be binary pebble bed is compared with the

experimental results as shown in Fig. 3.7 and Fig. 3.8 (normalized at zero MPa). Fig. 3.8 shows that the correlation obtained above for binary pebble bed does not differ so much from the measured correlation for single size pebble bed. However quantitative investigation can not be conducted from these figures because of the difference in packed mode (binary, single size) and pebble material (Be, Al).
Some supplements are given here as for the weighting function. The integration of Eq. (3.8) should intuitively be done using d(ln(r)) because the measured temperature distribution may be fitted with the logarithmic axis as shown in Fig. 3.1. Then the weighting function is selected as "1/r" on the contrary to the previous "r" as described below.

$$d(\ln(r)) = \frac{\partial \ln(r)}{\partial r} dr = \frac{1}{r} dr \qquad \text{---------- (3.18)}$$

With the weighting function (1/r), σ_{avg} may be calculated to be larger than previous value because the stress in inner region is lager than that in outer region. Further study is needed for the weighting function.

2) Heat transfer coefficient
The relation between compressive stress and $\Delta L/L$ for heat transfer coefficient can be obtained as follows:

$$\frac{\Delta L}{L} = \frac{(\Delta L / L)_{avg}}{(\sigma_r)_{in}} \times \sigma \qquad \text{---------- (3.19)}$$

$(\Delta L/L)_{avg}$: $\Delta L/L$ defined in Eq. (3.2)
$(\sigma_r)_{in}$: analyzed inner wall compressive stress
(Heat transfer coefficient is measured for only inner wall.)

From the analysis, next correlation is obtained.

○Case for minimum cap position = 1MPa

$$\frac{\Delta L}{L} = \frac{0.0927}{2.45} \times \sigma \qquad (\sigma \leqq 2.45 \text{ MPa}) \qquad \text{---------- (3.20)}$$

○Case for minimum cap position = 0.1MPa

$$\frac{\Delta L}{L} = \frac{0.0927}{0.969} \times \sigma \qquad (\sigma \leqq 0.969 \text{ MPa}) \qquad \text{---------- (3.21)}$$

Using the above equations, value of f in Eq. (3.2) is calculated as described below and the correlation between the heat transfer coefficient and compressive stress near wall is obtained with this value.

○Case for minimum cap position = 1MPa

with $f = 4.023 + 2.067 \times \sigma$ for $\sigma \geq 0.40[MPa]$
and $f = 1$ for $\sigma < 0.40[MPa]$
($\sigma \leqq 2.45$ MPa)

○Case for minimum cap position = 1MPa
with $f = 4.023 + 5.226 \times \sigma$ for $\sigma \geq 0.16[MPa]$
and $f = 1$ for $\sigma < 0.16[MPa]$
($\sigma \leqq 0.969$ MPa)

With the above correlation, the modified thermal conductivity for heat transfer (Eq. (3.4)) is calculated as shown in Fig. 3.9. Though there is a radical change in the thermal conductivity at $\sigma = \sim 0.4$MPa, due to the definition by Eq. (3.2) of no compressive effect for $\Delta L/L$ less than 0.015%, a linear change shown by a dotted line in the figure is assumed for convergence in computation. Thermal conductivity at near wall element is shown as a function of temperature in Fig. 3.10 and Fig. 3.11 for two minimum cap positions, respectively.

Table 3.1 Mechanical data for analysis of heat transfer experiment

d) Elastic constant

Young's modulus, E	1.45* GPa
Poisson's ratio, ν	0.25

e) Shear failure data

cohesion, d	0.5 / 0.05 MPa
friction angle, β	37.6°
parameter for cap center shift, R	0.5**
initial plastic volume strain, $\varepsilon_{vol}^{Pl}(0)$	0. ***
parameter for transition surface, α	0. **
yield stress ratio (tension/compression), K	1. **

f) Cap hardening data

No.	p(MPa)	ε_{vol}^{Pl}	Comment
1	1. / 0.1	0.	minimum cap position
2	29.	0.1	

*: Estimated by an analytic model of K. Walton [8] (Appendix A)

**: Typical values are temporary assumed based on ABAQUS/Standard user's manual [6].

***: No initial plastic volume strain is assumed.

Table 3. 2 Young's modulus of Be pebble bed

Item	FZK experiment	Breeding blanket
porosity, Φ	0.192 [5]	0.192 [5]
temperature, T	50 ℃	300 ℃
Young's modulus for Be bulk, E	295 GPa	281GPa
Poisson's ratio, ν	0.07	0.07
contacts per sphere, η	6.4 [9]	6.4 [9]
axial strain, ε	0.001*	0.001*
Young's modulus for Be pebble bed, E	1.45 GPa**	1.38 GPa**
inclination of cap hardening line E(cap)	0.29 GPa***	0.28 GPa***

* : Uniaxial strain is assumed

**: Estimated with the analytic model developed by K. Walton [8] (Appendix A). Temporarily assumed as single size pebble bed due to the lack of data for binary pebble bed.

*** : Assumed as 1/5 of pebble bed Young's modulus

Q_0 : 9.87 [W/cm^2]	(heat flux at the inner wall)
T : 50.8 [°C]	(average temperature of the bed)
P : 1.0 [bar]	(helium pressure)
λ : 12.07 [w/mK]	(thermal conductivity of the bed)
h : 0.94 [W/cm^3]	(heat transfer coefficient)

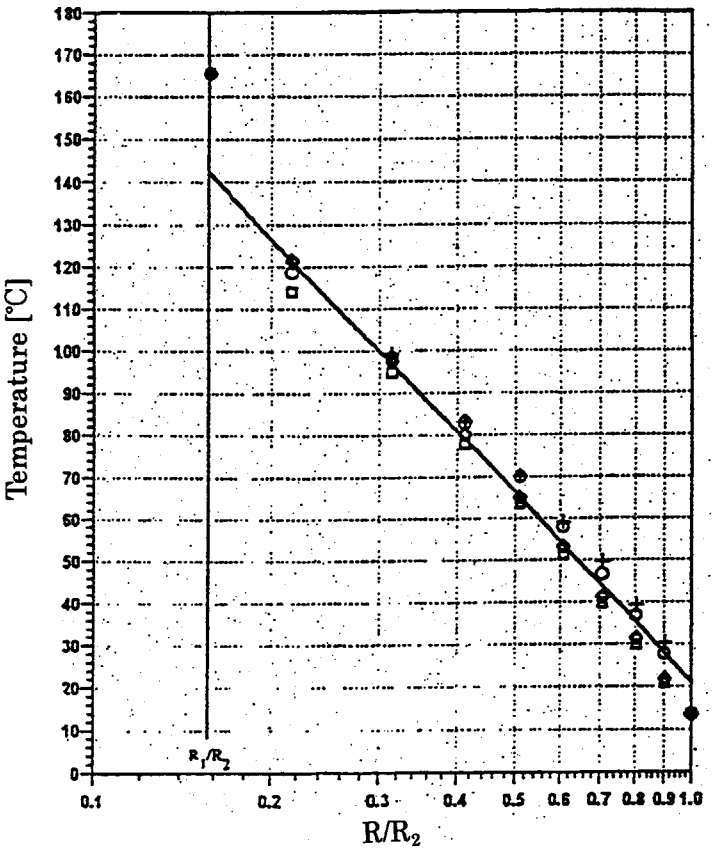

Fig. 3.1 Radial temperature distribution in the bed [5]

A) Experiment system (Cross-section of test equipment)

(The thickness of inner and outer tubes
is assumed to be 2 mm each.)

$\Delta L/L=0.0927$
(evaluated by Eq. 3.3)
$\alpha_{Be} = 1.4\times10^{-5}$
$\alpha_{SS} = 1.6\times10^{-5}$

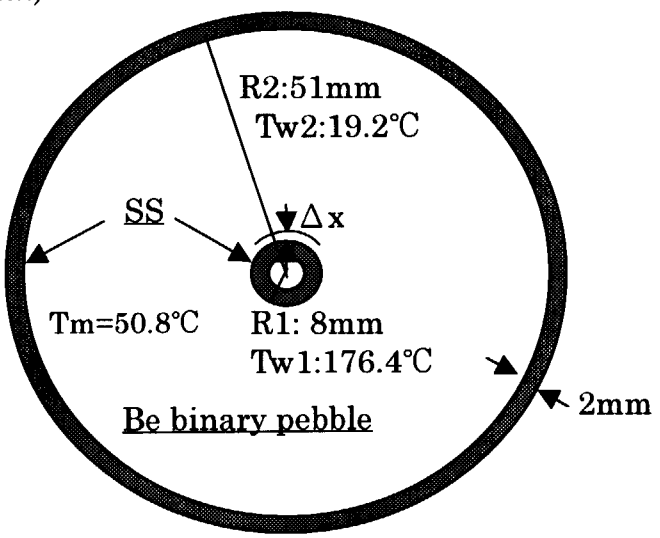

B) Analysis model
○2D cylindrical

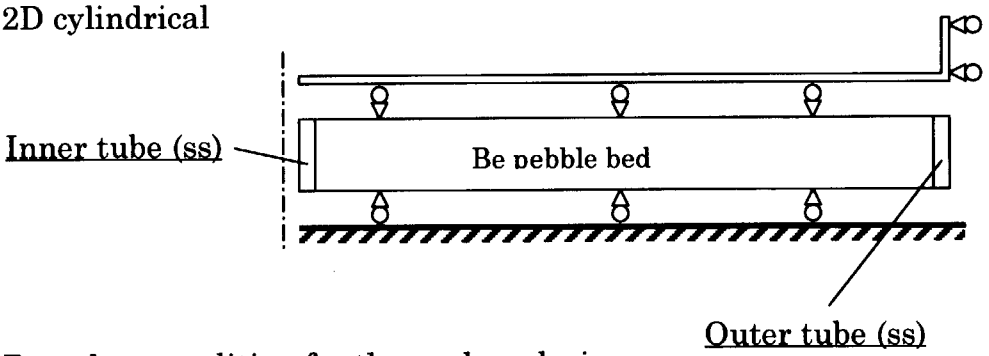

Boundary condition for thermal analysis :
inner surface of inner tube (SS) : 180℃
outer surface of outer tube (SS) : 18℃
(This condition is estimated with experimental temperature distribution in Fig. 3.1)

Fig. 3.2 Analysis model of FZK experiment system

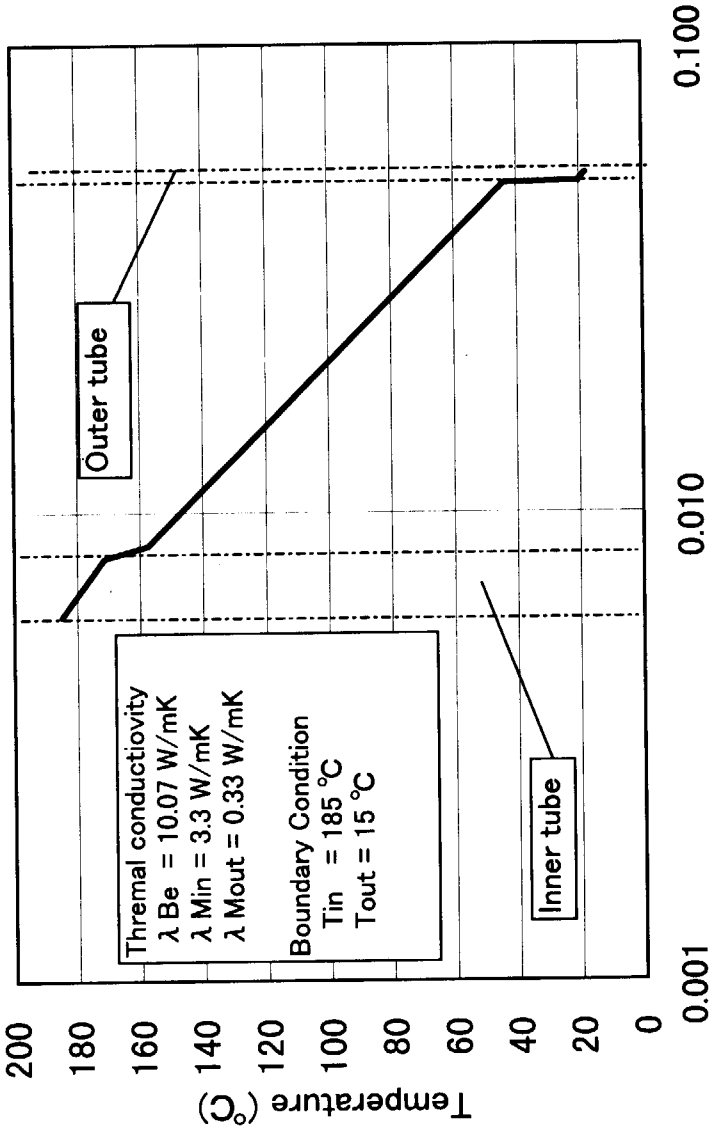

Fig. 3.3 Analyzed temperature distribution of the heat transfer experiment
(Constant thermal conductivity)

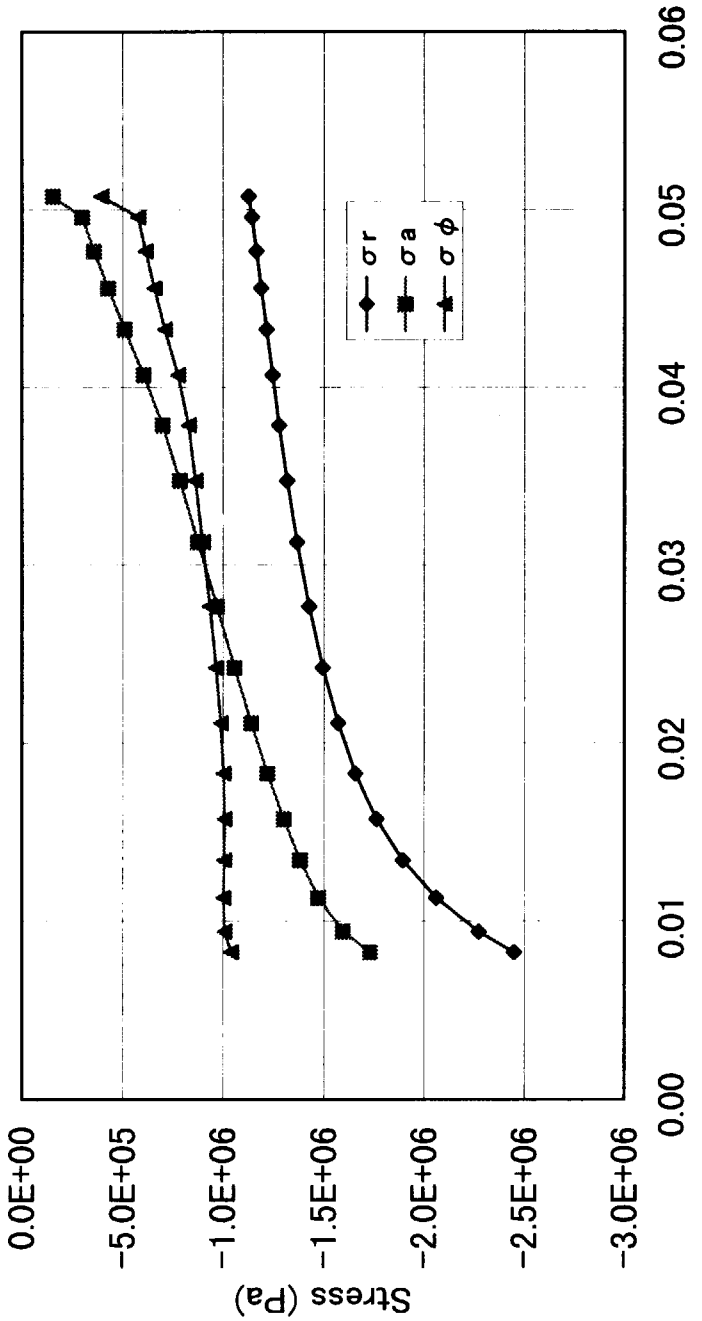

Fig. 3.4 Analyzed stress distribution in the heat transfer experiment (Minimum cap position = 1MPa)

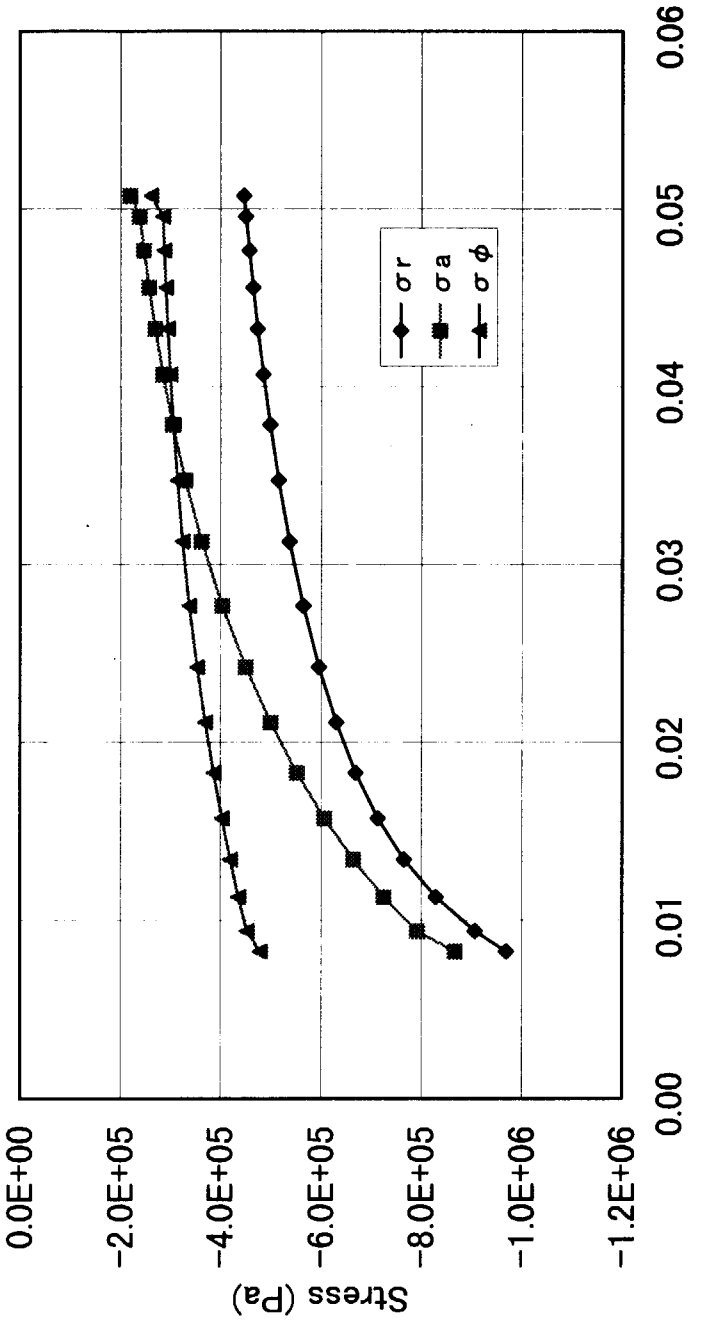

Fig.3.5 Analyzed stress distribution in the heat transfer experiment (Minimum cap position = 0.1MPa)

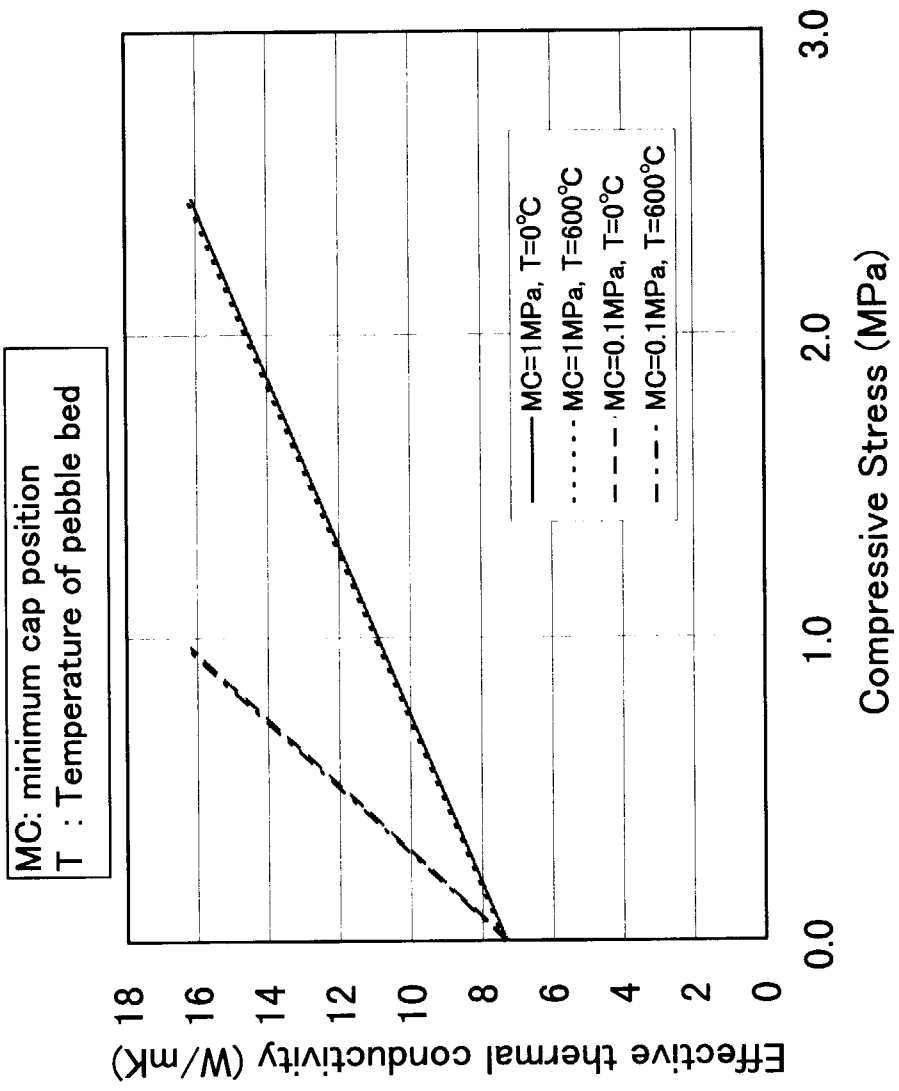

Fig. 3.6 Evaluated relation between effective thermal condcutivity and compressive stress (Be binary pebble bed)

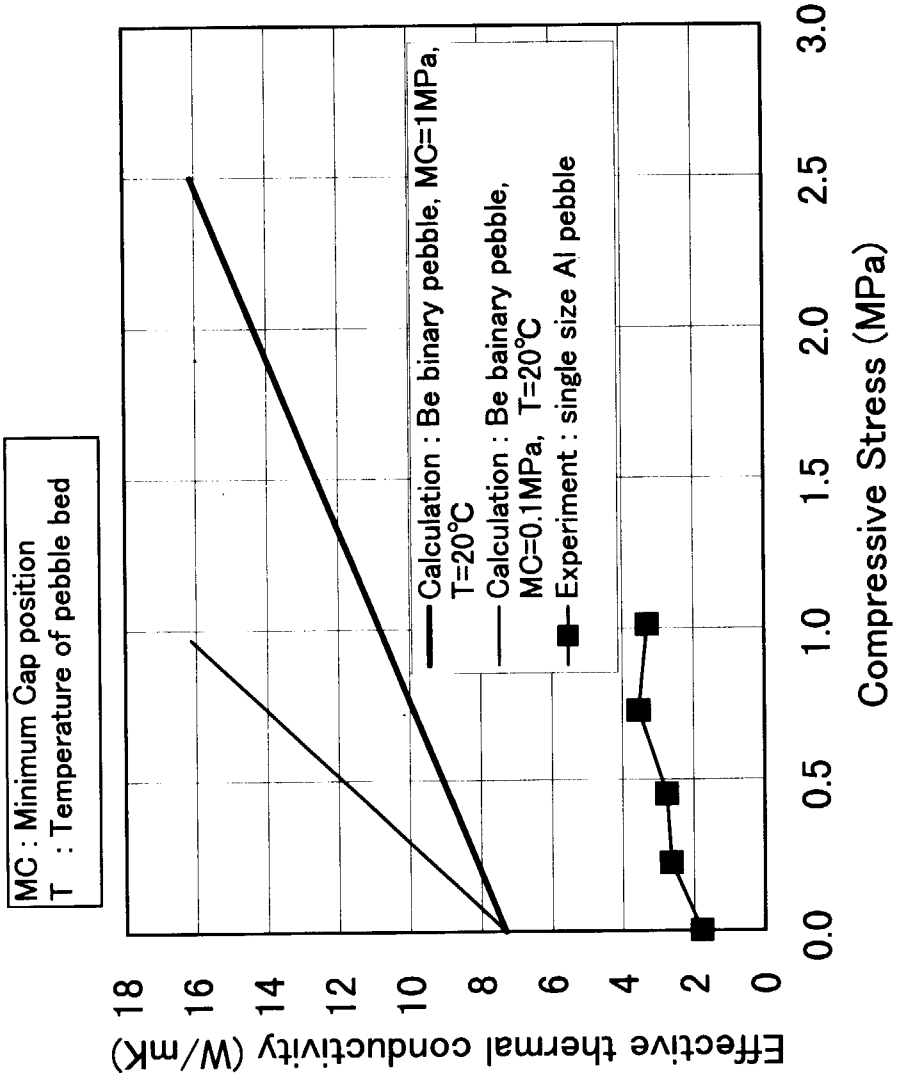

Fig. 3.7 Comparison of relations between effective thermal condcutivity and compressive stress

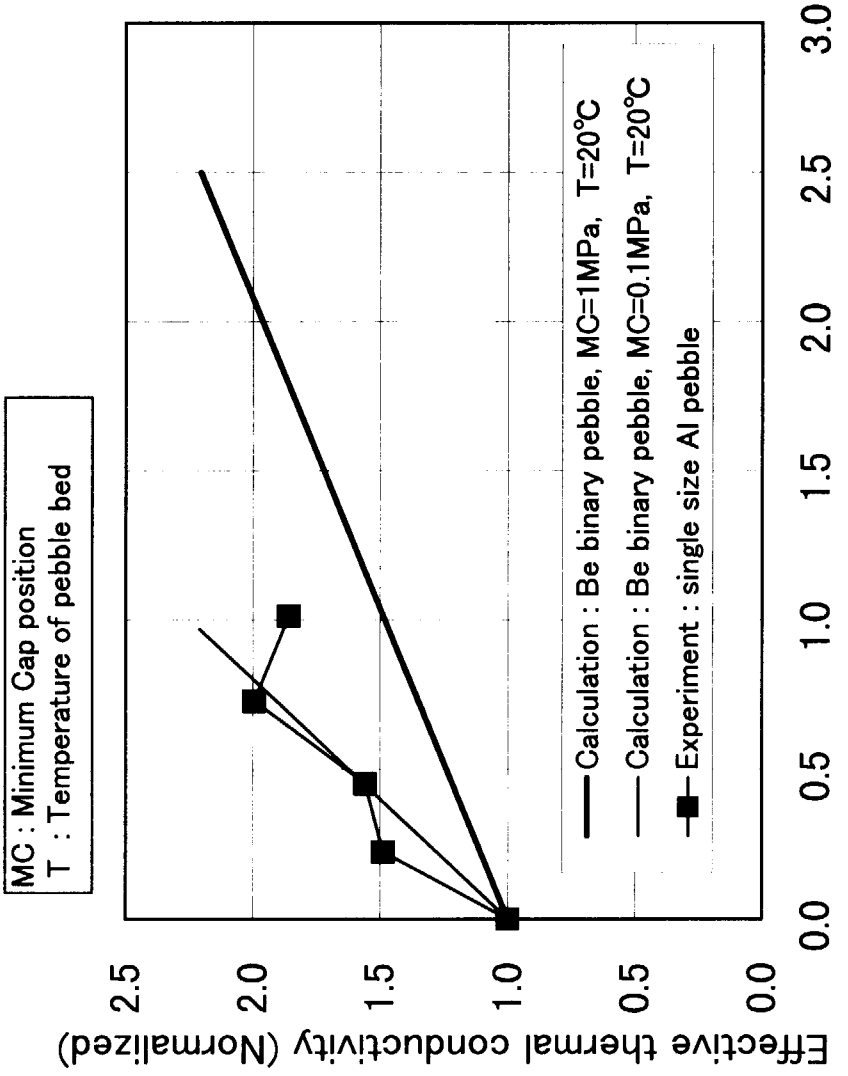

Fig. 3.8 Comparison of relations between normalized effective thermal condcutivity and compressive stress

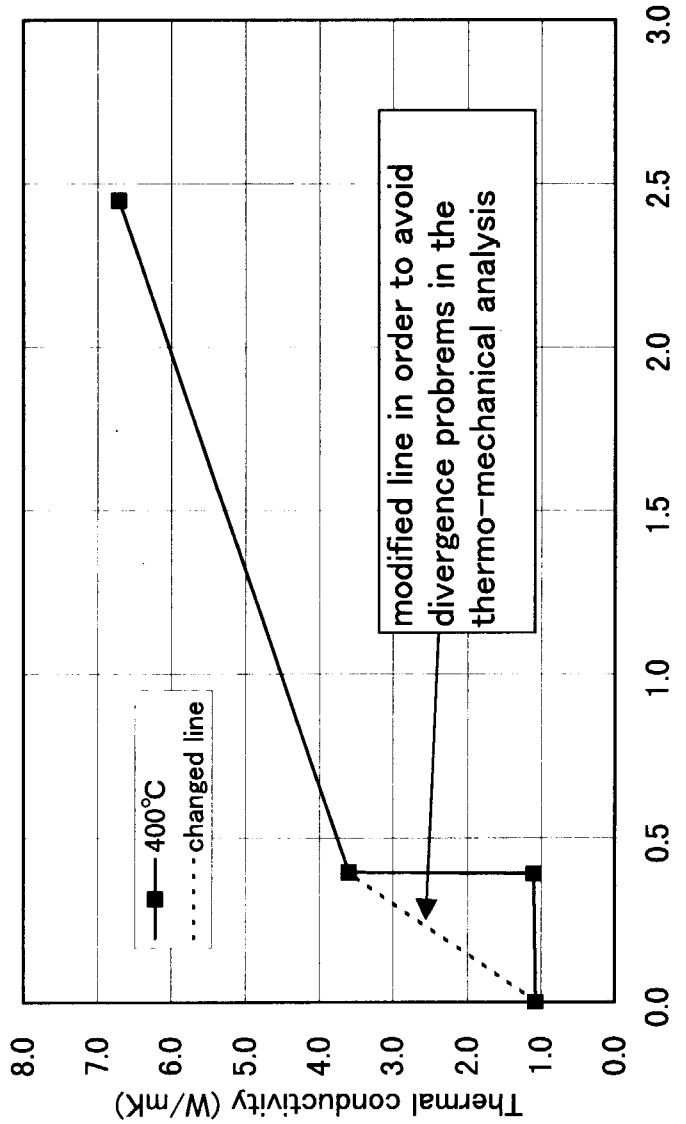

Fig. 3.9 Modification in relation between thermal conductivity for heat transfer and compressive stress (Minimum cap position=1MPa)

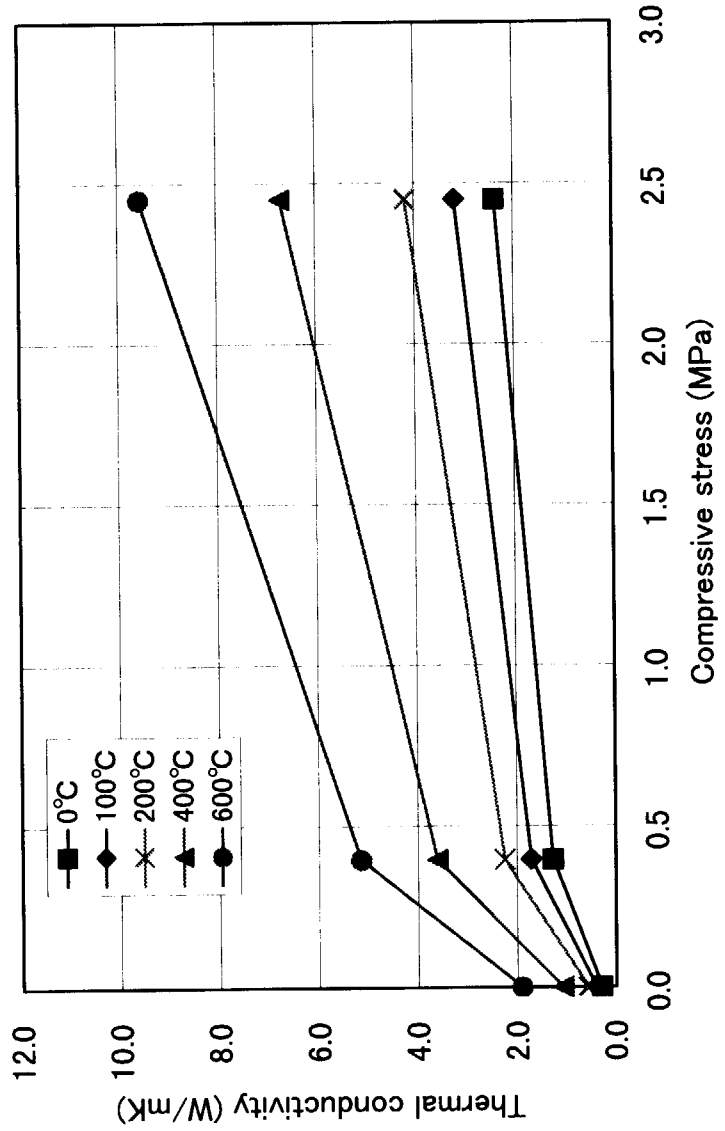

Fig. 3.10 Relation between modified thermal conductivity for heat transfer and compressive stress (Minimum cap position=1MPa)

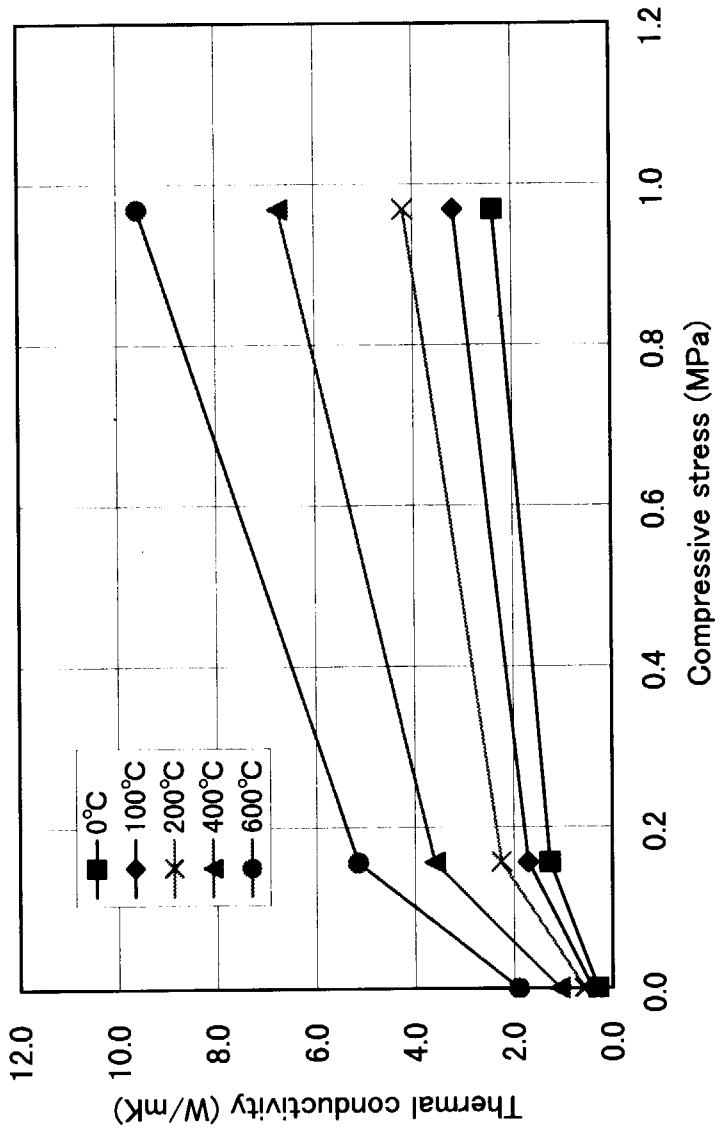

Fig. 3.11 Relation between modified thermal conductivity for heat transfer and compressive stress (Minimum cap position=0.1MPa)

4.Thermo-mechanical Analysis Method

4.1 Analysis Method

The coupled temperature-displacement analysis procedure of ABAQUS code is selected as shown in Fig. 4.1 in order to take into account the dependencies of thermal conductivity and heat transfer coefficient on compressive stress. Thermal conductivity is automatically calculated based on the iterated stress (σ) at every calculation point.

4.2 Verification of Thermo-mechanical Analysis

The heat transfer experiment [5] is analyzed with the coupled temperature-displacement analysis procedure using correlation obtained in 3.3 and the same mechanical data as in 3.3 (Table 3.1). Analyzed thermal conductivity distribution and temperature distribution are shown in Fig. 4.2 and Fig. 4.3, respectively. In comparison with the previous thermal analysis results (Fig. 3.3), the temperature jump at the outer wall surface is reduced to the same magnitude as the experimental results in Fig. 3.1. Because of the reduction of the temperature jump, the averaged temperature in the pebble bed becomes lower than the case without the effect of compressive stress on effective thermal conductivity. The temperature distribution in the pebble bed region shows slight convex curvature since the thermal conductivity of outer region is lower than that of more compressed inner region. The convex curvature can be also seen for the measured temperature distribution plotted in Fig. 3.1, which may demonstrate the compressive effect on the thermal conductivity. The analyzed stress distribution in the pebble bed is shown in Fig. 4.4 and Fig. 4.5. The analyzed stress is lower than the case without compressive effect because of its lower temperature.

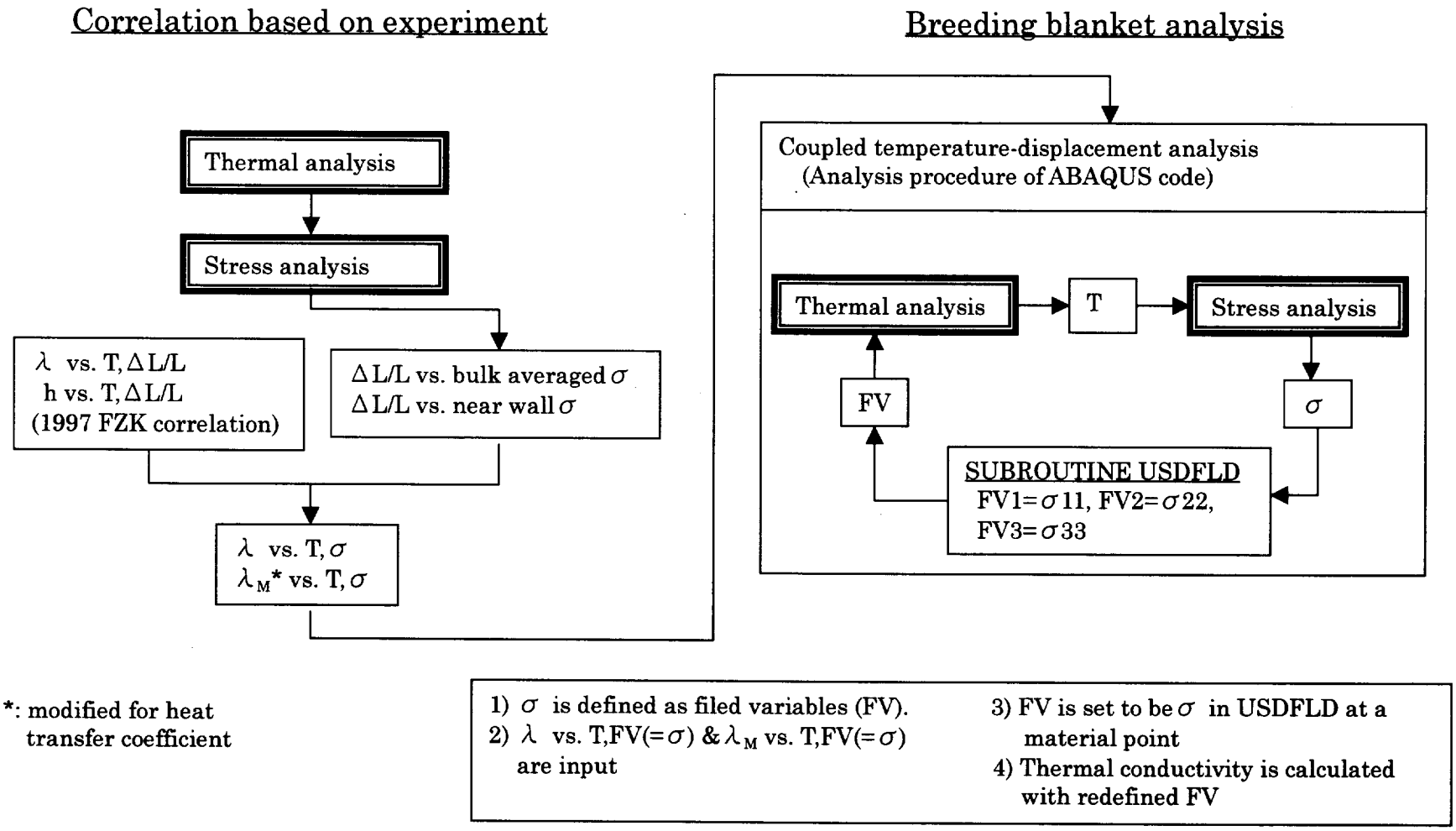

Fig. 4.1 Flow of thermo-mechanical analysis of breeding blanket

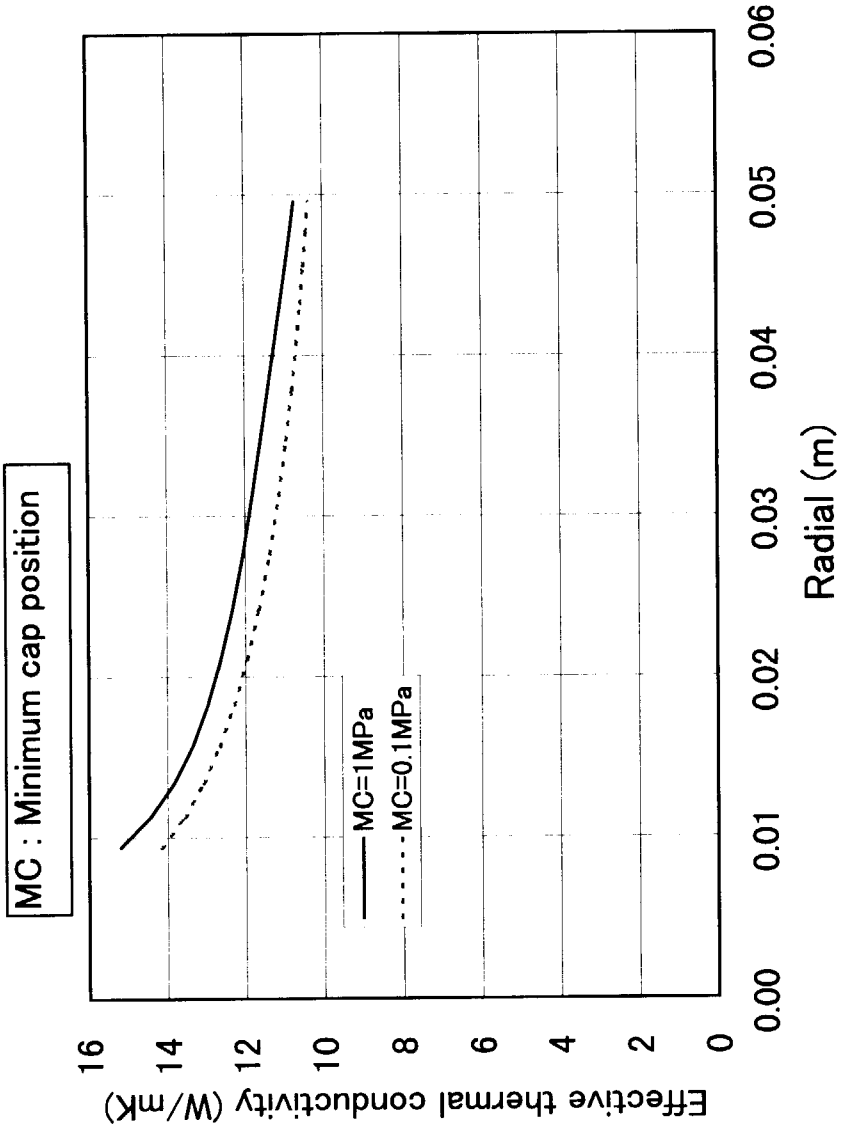

Fig. 4.2 Evaluated distribution of effective thermal conductivity in the heat transfer experiment system

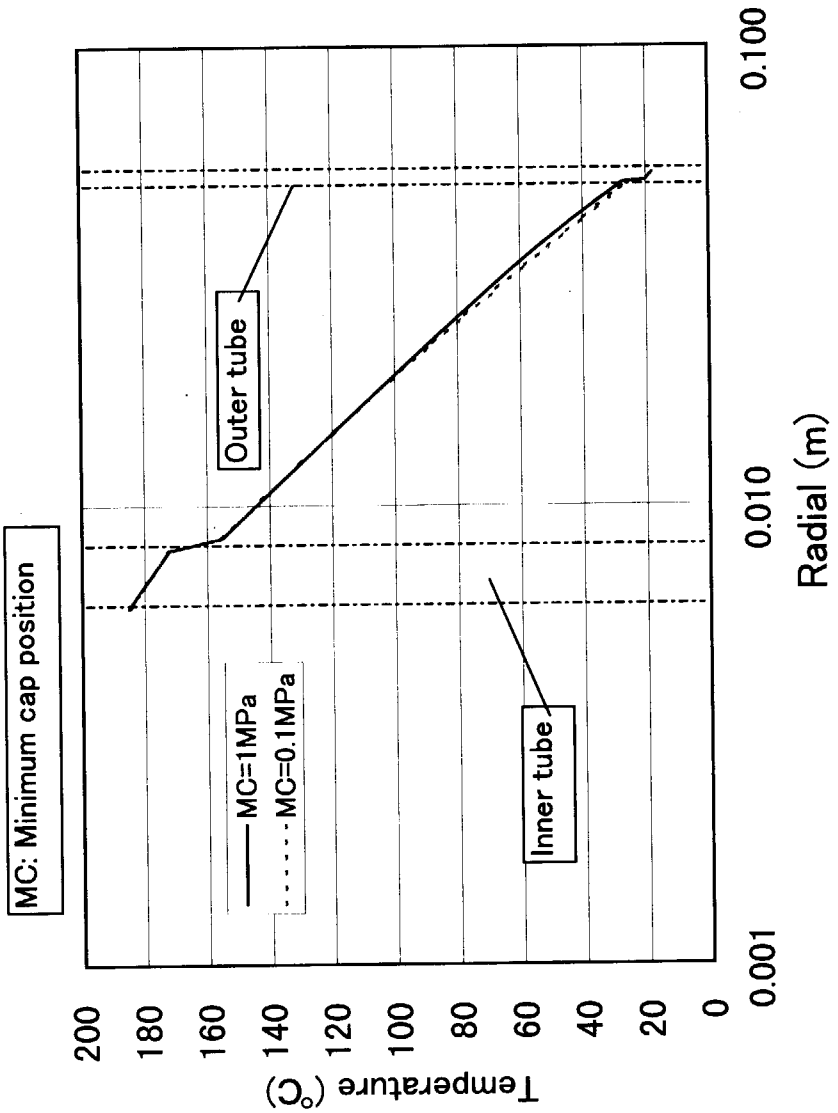

Fig. 4.3 Analyzed temperature distribution with coupled temperature-displacement procedure

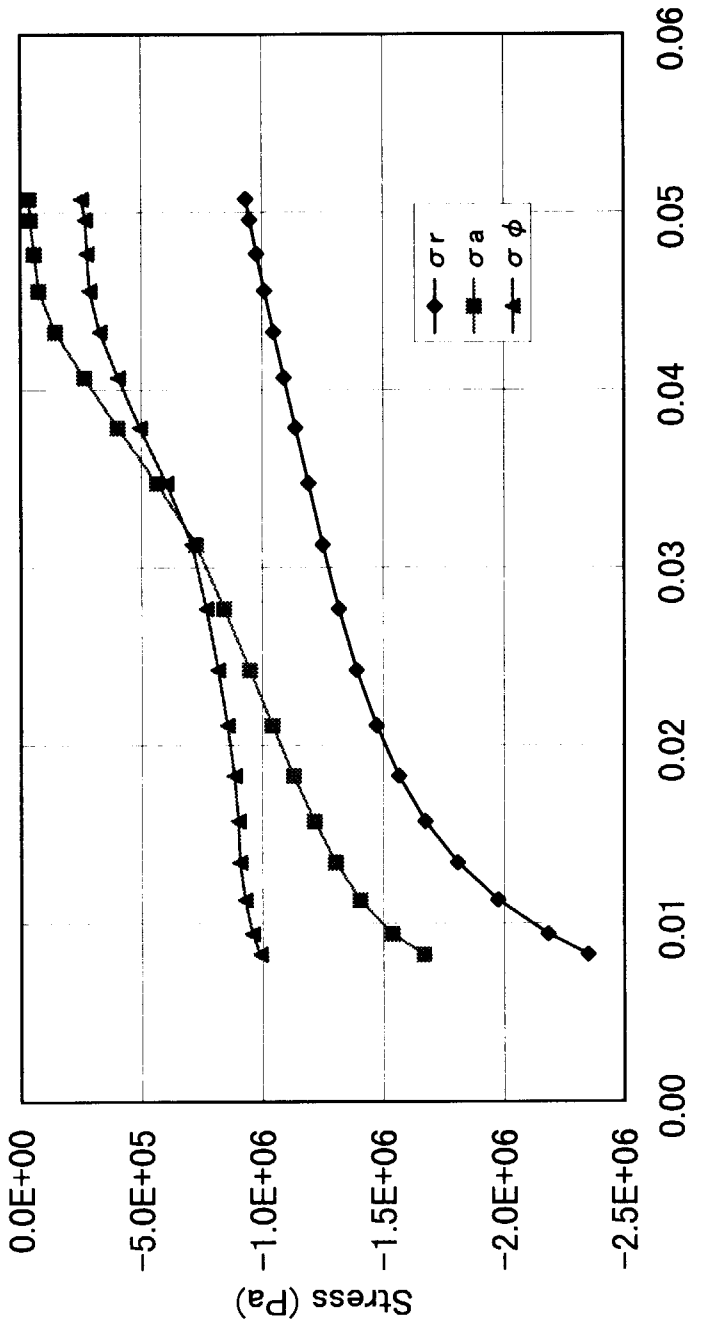

Fig. 4.4 Analyzed stress distribution with coupled temperature-displacement procedure (Minimum cap position = 1Mpa)

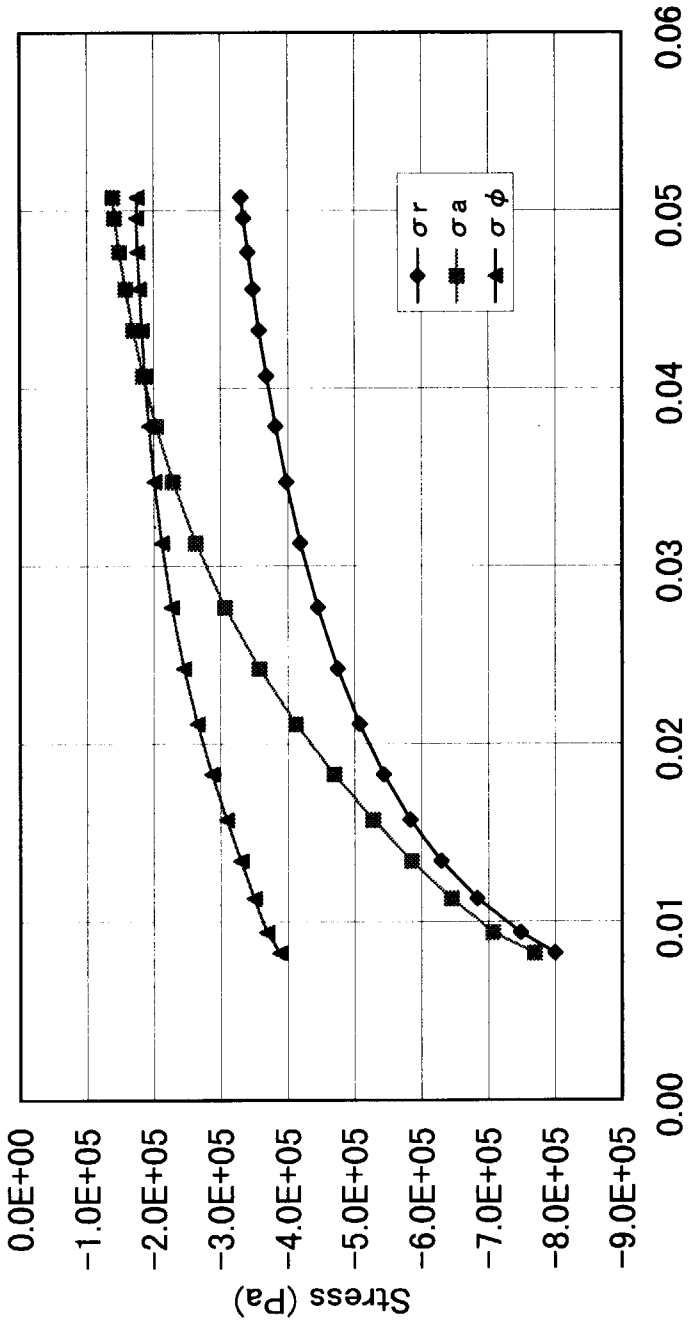

Fig. 4.5 Analyzed stress distribution with coupled temperature-displacement procedure (Minimum cap position = 0.1Mpa)

5. Analysis of Breeding Blanket

Thermo-Mechanical analysis is conducted on ITER breeding blanket by the method and data discussed above.

5.1 Analysis Condition

1) Analysis case

- Unit cell of ITER #19 (outboard mid-plane) breeding blanket (Fig. 5.1)
  - Case A: nominal case with effective thermal conductivity of Be pebble bed dependent on the stress
  - Case B: constant thermal conductivity in the Be pebble bed bulk region (λ = 13.43 W/mK) (referred from [1])
  - Case C: λ = -20% of nominal case in the Be pebble bed bulk region
  - Case D: λ = +20% of nominal case in the Be pebble bed bulk region

2) Analysis model

- Unit cell of ITER #19 (outboard mid-plane) breeding blanket
- 2D X-Y model with plane strain elements as shown in Fig. 5.2. (Generalized plane strain condition is desirable but unavailable for the Coupled Temperature-Displacement analysis at present.)

3) Analysis code / model

- ABAQUS5.7 / modified DRUCKER-PRAGER/Cap plasticity model

(Coupled Temperature-Displacement analysis procedure was for case A, C and D)

4) Thermal data

a) Thermal loading [1]

- Heat flux	first wall	0.5 MW/m^2
- Volumetric heating	Be	6.63*EXP(-6.41*X) MW/m^3
	Li_2ZrO_3	Table 5.3
	SS316LN	9.52*EXP(-5.085*X) MW/m^3
		(X: distance from first wall)

b) Heat transfer coefficient (h), coolant temperature (T) [1]

- First wall channel	h=27400 W/m^2 K, T=145°C
- Cooling plate channel	h=13000 W/m^2 K, T=170°C
- Cooling plate header	h=22000 W/m^2 K, T=190°C

c) Pebble bed effective thermal conductivity

Be pebble bed

Case A:

Among two thermal conductivity correlations described in 3.2, the correlation for the minimum cap position of 0.1 MPa (Eq. (3.17)) failed to converge in the analysis. Therefore one for the minimum cap position of 1MPa (Eq. (3.16)) is used here. At smaller compressive stresses than 0 MPa, the effective thermal conductivity is set as 7.31 W/mK corresponding to a value at 0 MPa. At lager ones than 2.45 MPa, the effective thermal conductivity is set as 16.12 W/mK corresponding to a value at 2.45 MPa which is the maximum stress of the analyzed heat transfer experimental system. Between the two compressive stresses, thermal conductivity is estimated by Eq. (3.16).

Case B:

13.43 W/mK

Case C:

-20% of case A

Case D:

+20% of case A

Li_2ZrO_3

Effective thermal conductivity of Li_2ZrO_3 pebble bed is estimated with SZB analytic model [10] as shown in Fig. 5.3. The effect of compressive stress on the effective thermal conductivity is not taken into account because it is reported that the compressive effect has not been significantly observed for Li_2ZrO_3 pebble bed in the experiment [7].

Calculation condition:

Li_2ZrO_3 pebble bed	$2\phi(65\%)+0.2\phi(15\%)$
SZB model	Contact area = 0.
	Accommodation factor=0.4

d) Modified thermal conductivity for near wall element to take heat transfer coefficient at wall into account

Be pebble bed

The modified thermal conductivity described in section 3.3, 2) is used in case A, C and D. The used thermal conductivity is shown in Fig. 3.10. In case B, heat transfer coefficient is not taken into account.

Li2ZrO3 pebble bed

The heat transfer coefficient between Li_2ZrO_3 pebble bed and the tube wall was not taken into account at present.

e) Thermal expansion coefficient of pebble bed

The same values as base materials (Be, Li_2ZrO_3) as shown in Table 5.1 are used.

5) Mechanical data

Mechanical data for the cap model analysis are summarized in Table 5.2.

a) Young's modulus

Be pebble bed

The Young's modulus for Be single size pebble bed is tentatively applied, which is estimated as 1.38 GPa by the analytic model of K.Walton in the same way as described in the section 3.2.1, 5). This value is slightly less than that used in the analysis of the heat transfer experimental system because of higher temperature of the breeding blanket as shown in Table 3.2.

Li2ZrO3

The Young's modulus used here is 0.5 GPa which is experimentally obtained for Li_2ZrO_3 single size pebble bed at axial compressive strain = nearly 0.3% [4].

b) Cap hardening data

Be pebble bed

Minimum cap position is assumed to be 1 MPa. Another cap hardening pressure is determined as shown in Table 3.2 based on the inclination of cap hardening line assumed as 1/5 of Young's modulus.

Li2ZrO3

Minimum cap position is assumed to be 1 MPa. Another cap hardening pressure is determined with the inclination of cap hardening line calculated using Fig. 5.4 in which 1st loading and 1st unloading lines are drawn based on Fig. 2.5.

$$p = \frac{1}{3}(\sigma_{a1} + 2\sigma_r) = \frac{1}{3}(1 + 2k_0)\sigma_{a1} = 2.1MPa \qquad \text{---------- (5.1)}$$

p : hydrostatic pressure

ε_{a1}, ε_{a2} : axial strain (0.0105, 0.006 ; Fig. 5.4)

σ_{a1} : axial stress (3.8MPa ; Fig. 5.4)

ν : Poisson's ratio (0.25 [4])

k_0 : $=\sigma_r/\sigma_a$ (0.339; temporarily assumed to be the same as that for Al pebbles because of no available data for Li_2ZrO_3 at present)

$\varepsilon_{vol}^{Pl} = \varepsilon_{a2} = 0.006$

Since the inclination of Cap hardening line is calculated as 350 MPa (=2.1MPa/0.006), the hydrostatic pressure is 350 MPa at $\varepsilon_{vol}^{Pl} = 1$.

c) Shear failure data

The shear failure data are the same as those used in section 3.1 (Table 2.1) except for the friction angle. The friction angle used here is 30.6° for 2-D X-Y model with plane strain condition.

5.2 Results of Analysis

1) Case A (nominal case)

The analyzed temperature distribution is shown in Fig. 5.5. The maximum and minimum temperatures of breeding material (Li_2ZrO_3) are summarized for each breeder tube in Table 5.3. The maximum temperatures for other materials are also summarized in Table 5.4. In the design of the breeding blanket, temperature limits are tentatively considered to be within 300-350℃ to 800℃ for Li_2ZrO_3 and under 500℃ for Be [1].

The temperature of the breeding material ranges from 317℃ (No. 8 breeder tube) to 554℃ (No. 6 breeder tube). Since the heat transfer coefficient between the breeder pebbles and the tube surface are not taken into account in this analysis, the temperature would become slightly higher with this effect, but would be still within the limits. The maximum temperature of Be pebble region is 446℃ which is below the present limit (500℃).

The stress distributions in the X and Y directions are shown in Figs. 5.6 and 5.7, and the minimum and maximum stresses are summarized in Table 5.5. Tensile stress is found in the entire breeding region because the thermal expansion coefficient of Li_2ZrO_3 is less than that of tube material (SS). The stress in the Be pebble region spatially varies from -2.5MPa to 0.47MPa as shown in Table 5.5. Strong compressive force is generated in the higher temperature region, so compressive stresses in the region near the first wall and far from the cooling panel are higher than the other region.

Stresses in SS (first wall, tube, rib and back wall) are extremely high because of the plane-strain condition. However, the plane-strain condition is impractically severe, and it is desirable that the code would be improved to apply generalized plane-strain condition.

2) Case B (case for constant thermal conductivity)

Analyzed temperature and stress distributions are shown in Figs. 5.8-5.10. These are similar to the results of the nominal case (case A) as also seen from Table 5.3-5.5.

Slight difference from the nominal case, the temperatures of the 8th breeder tube and the shielding plate of case A are higher than those of case B. case, is found. This feature is appreciated by the compressive effect. In case A the compressive stresses in the Be pebble bed region located between 8th (last) breeder tube and shielding plate are lower than the other region as shown in Figs. 5.11 and 5.12 where stress distributions are drawn focusing on Be pebble bed. The lower compressive stresses cause the thermal conductivity of the region lower and then the temperature higher.

Consequently it might be concluded that the spatially constant thermal conductivity estimated by FZK (Eq. 3.1)) is fairly good as a whole for ITER type breeding blanket. Naturally detailed treatment of tmermo-mechanical property including spatially varying thermal conductivity depending on the stress is required for accurate analysis, particularly in the case of time dependent thermo-mechanical analysis

3) Case C, D (case for conductivity of $\pm 20\%$)

Analyzed temperature and stress distributions are shown for case C and D in Figs. 5.13-5.18. The temperatures of the breeding material (Li_2ZrO_3 pebble bed) for case C (λ_{Be}=-20%) are about 20-30℃ higher than those for case A (nominal) as shown in Table 5.3. The maximum temperature of the multiplier (Be pebble bed) for case C are 45℃ higher than that for case A. The temperatures for case D (λ_{Be}=+20%) are about 12-16℃ lower in the Li_2ZrO_3 pebble bed and 31℃ lower in the Be pebble bed.

Current design of ITER breeding blanket is evaluated to permit $\pm 20\%$ change in thermal conductivity of Be pebble bed.

For more detail quantitative estimates of the breeding blanket, further studies are required as for:

- elaborate investigation of thermal and mechanical properties of binary pebble bed, including pebble-wall friction and behaviors of pebbles subjected to tensile stresses
- establishment of analysis methods and constitutive equation to describe these pebbles behavior based on plastic theory
- incorporation of the analysis method and the constitutive equation into available thermo-mechanical analysis code

Table 5.1 Thermal expansion coefficient

(1/K)

T(℃)	SS[11]	Be[11]	Li2ZrO3[12]
20	1.59E-05	1.13E-05	9.92E-06
50	1.61E-05	1.19E-05	9.93E-06
100	1.64E-05	1.29E-05	9.93E-06
150	1.67E-05	1.38E-05	9.94E-06
200	1.70E-05	1.47E-05	9.94E-06
250	1.72E-05	1.55E-05	9.95E-06
300	1.75E-05	1.63E-05	9.95E-06
350	1.77E-05	1.70E-05	9.96E-06
400	1.79E-05	1.77E-05	9.97E-06
450	1.81E-05	1.83E-05	9.97E-06
500	1.83E-05	1.88E-05	9.98E-06
550	1.85E-05	1.94E-05	9.98E-06
600	1.87E-05	1.99E-05	9.99E-06

Table 5.2 Mechanical data for analysis of breeding blanket

g) Elastic constant

	Be	Li2ZrO3
Young's modulus, E	1.38 GPa	0.5 GPa
Poisson's ratio, ν	0.25	0.25

h) Shear failure data

	Be	Li2ZrO3
cohesion, d	0.5 MPa	0.5 MPa
friction angle, β	30.6°	30.6°
parameter for cap center shift, R	0.5*	0.5*
initial plastic volume strain, $\varepsilon_{vol}^{Pl}(0)$	0. **	0. **
parameter for transition surface, α	0. *	0. *
yield stress ratio (tension/compression), K	1. *	1. *

i) Cap hardening data

(Three sets of hydrostatic compression pressure (p) and plastic volume strain ε_{vol}^{Pl}) are used, The third set is added because plastic volume strain may exceed that of the second set (0.1))

	Be		Li2ZrO3		
No.	p(MPa)	ε_{vol}^{Pl}	p(MPa)	ε_{vol}^{Pl}	Comment
1	1.	0.	1.	0.	minimum cap position
2	27.6	0.1	35.	0.1	
3	276.	1.	350.	1.	

*: Typical values are temporarily assumed based on ABAQUS/Standard user's manual [6].

**: No initial plastic volume strain is assumed.

Table 5.3 Analyzed temperature of bleeding material (Li_2ZrO_3)

Tube No.	Tube Radius (mm)	Power density (W/cm^3)	Case A (Nominal)		Case B λ_{Be}= 13.43 W/mK		Case C λ_{Be}=-20%		Case D λ_{Be}=+20%	
			Min.	Max.	Min.	Max.	Min.	Max.	Min.	Max.
1	4	45.5	362	513	349	506	380	537	350	497
2	4	39.2	372	527	372	527	404	561	363	504
3	4	36.8	376	522	370	523	402	556	360	498
4	4	34.9	363	500	355	499	386	532	348	478
5	4	32	364	482	355	479	389	514	348	461
6	6.5	20.2	348	554	331	544	372	587	333	532
7	6.5	15.5	337	506	306	477	362	538	321	483
8	6.6	10.9	317	448	277	404	340	478	302	427

Table 5.4 Analyzed maximum temperature of Armor(Be), multiplier (Be), structure (SS)

Region	Case A (Nominal)	Case B: λ_{Be}= 13.43 W/mK	Case C: λ_{Be}=-20%	Case D: λ_{Be}=+20%
Armor (Be)	290	290	290	290
Multiplier (Be)	446	455	491	415
Structure (SS)	444	449	486	532

Table 5.5 Analyzed stresses of breeding blanket

		Case A (Nominal)		Case B: λ_{Be}=13.43 W/mK		Case B: λ_{Be}=−20%		Case B: λ_{Be}=+20%	
		Min.	Max.	Min.	Max.	Min.	Max.	Min.	Max.
First wall (SS)	σ−X	−2.65E+07	1.42E+07	−2.48E+07	1.31E+07	−2.80E+07	1.50E+07	−2.54E+07	1.36E+07
	σ−Y	4.68E+08	5.93E+08	3.70E+08	4.88E+08	5.17E+08	6.44E+08	4.31E+08	5.55E+08
	σ−Z	−1.22E+09	−1.13E+09	−1.31E+09	−1.22E+09	−1.22E+09	−1.12E+09	−1.22E+09	−1.13E+09
	MISES	1.50E+09	1.54E+09	1.51E+09	1.55E+09	1.54E+09	1.58E+09	1.48E+09	1.52E+09
Multiplier (Be pebble)	σ−X	−2.52E+06	4.70E+05	−2.68E+06	4.90E+05	−2.99E+06	4.67E+05	−2.20E+06	4.71E+05
	σ−Y	−2.07E+06	1.35E+05	−2.37E+06	1.47E+05	−2.53E+06	1.23E+05	−1.74E+06	1.33E+05
	σ−Z	−3.33E+06	1.79E+05	−3.43E+06	1.89E+05	−3.83E+06	1.75E+05	−3.00E+06	1.73E+05
	MISES	3.24E+05	1.32E+06	3.38E+05	1.28E+06	3.33E+05	1.42E+06	3.28E+05	1.25E+06
Breeder (Li2ZrO3 pebble)	σ−X	1.11E+05	4.21E+05	1.11E+05	3.83E+05	1.25E+05	4.36E+05	1.01E+05	4.09E+05
	σ−Y	2.08E+05	4.11E+05	1.98E+05	4.02E+05	2.07E+05	4.27E+05	2.16E+05	3.98E+05
	σ−Z	−2.25E+05	8.34E+04	−2.49E+05	4.25E+04	−1.48E+05	1.11E+05	−2.80E+05	5.99E+04
	MISES	3.21E+05	4.63E+05	3.41E+05	4.75E+05	3.10E+05	4.36E+05	3.22E+05	4.86E+05
Structure (Tube, rib,back wall)	σ−X	−6.52E+07	7.08E+07	−6.48E+07	9.78E+07	−6.83E+07	7.75E+07	−6.28E+07	6.81E+07
	σ−Y	−3.08E+08	7.10E+08	−2.54E+08	5.88E+08	−3.18E+08	7.49E+08	−2.90E+08	6.81E+08
	σ−Z	−1.20E+09	−2.19E+08	−1.28E+09	−3.27E+08	−1.31E+09	−2.08E+08	−1.13E+09	−2.27E+08
	MISES	4.51E+08	1.19E+09	5.23E+08	1.26E+09	4.51E+08	1.29E+09	4.51E+08	1.11E+09

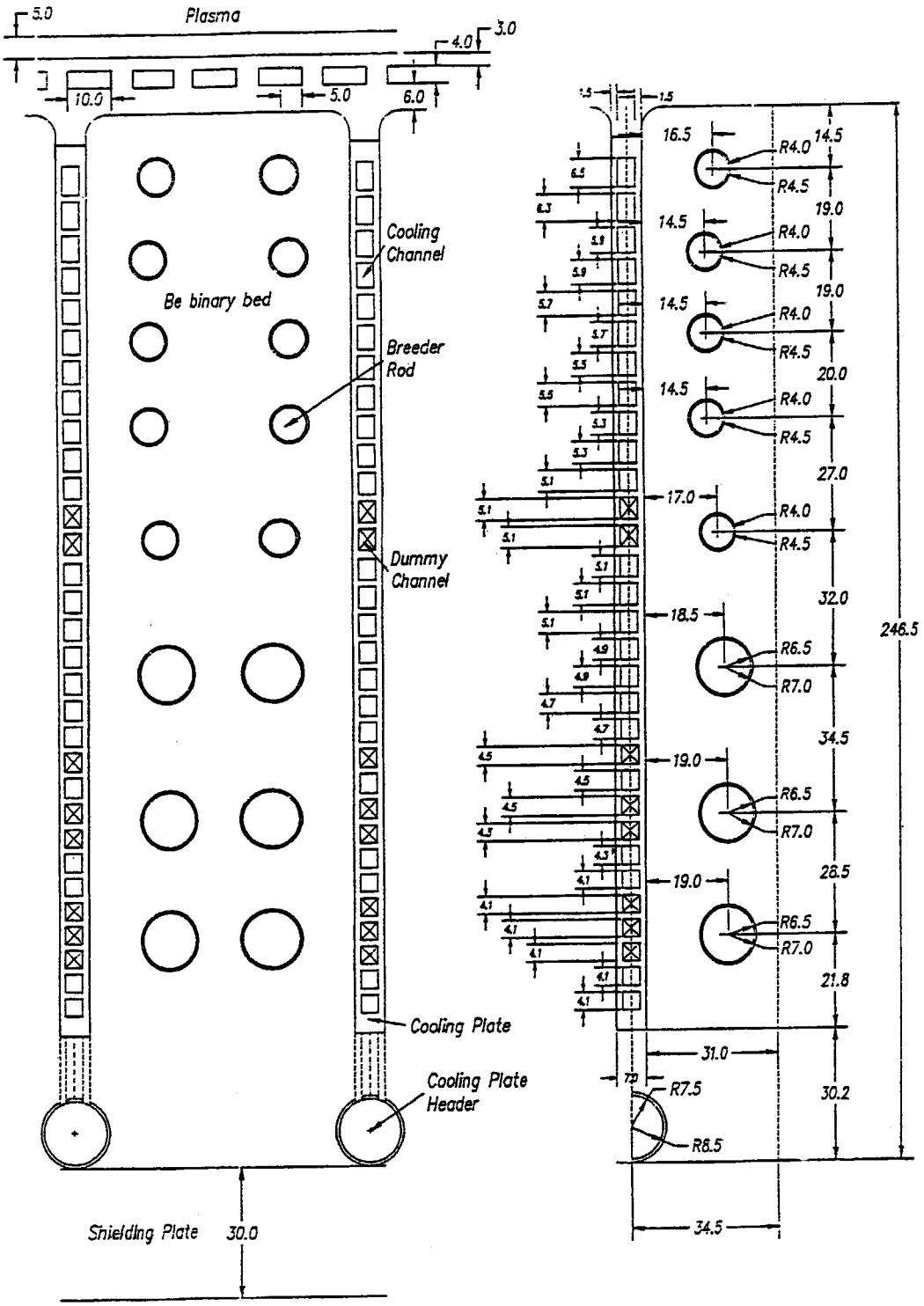

Fig. 5.1 Module #19 basic cell [1]

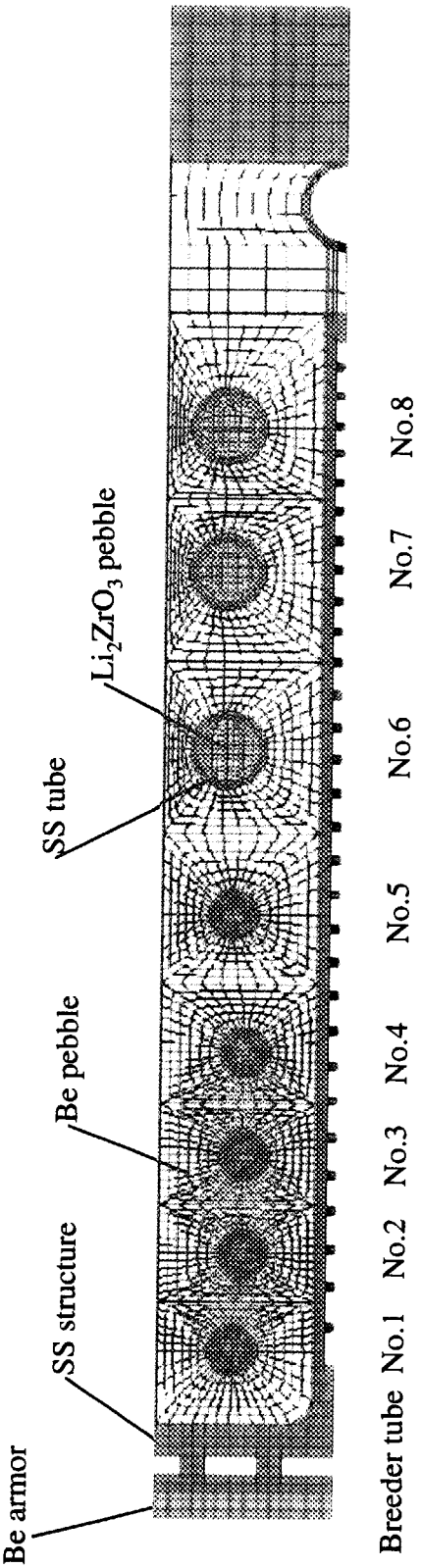

Fig. 5.2 Analysis model of ITER #19 breeding blanket

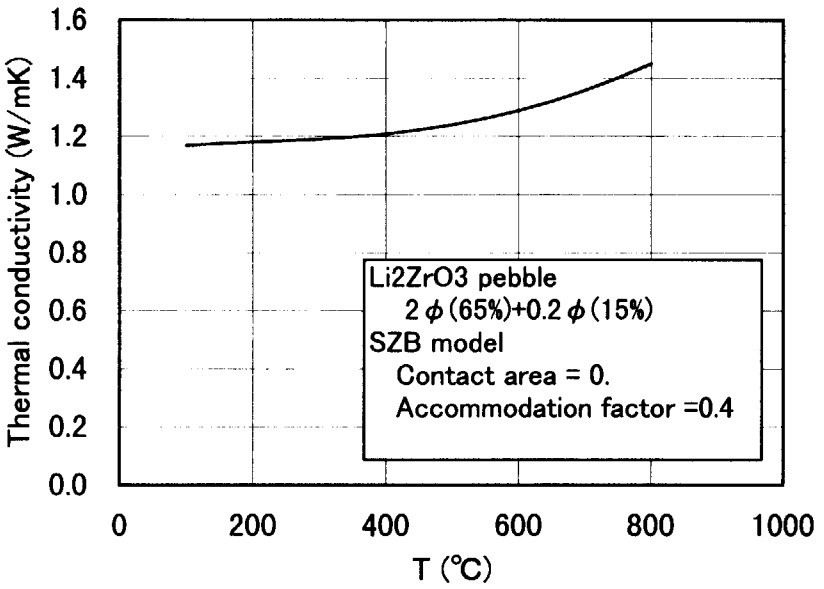

Fig. 5.3 Thermal conductivity of Li2ZrO3 binary pebble bed (Calculated with SZB model)

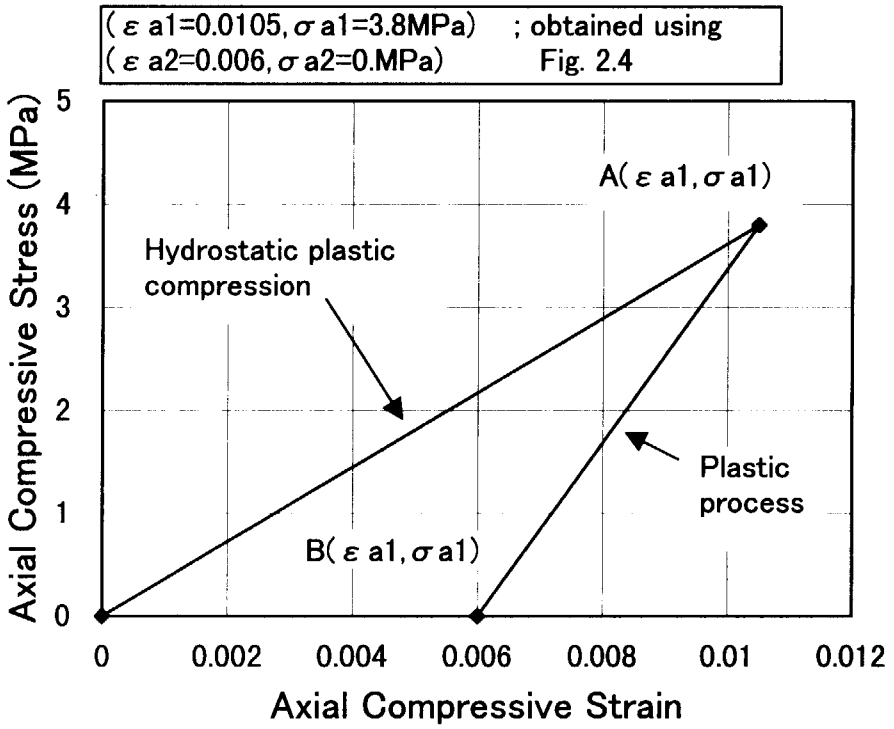

Fig. 5.4 Relation between the axial compressive strain and the axial compressive stress for Li2ZrO3 single size pebble bed based on Fig. 2.5

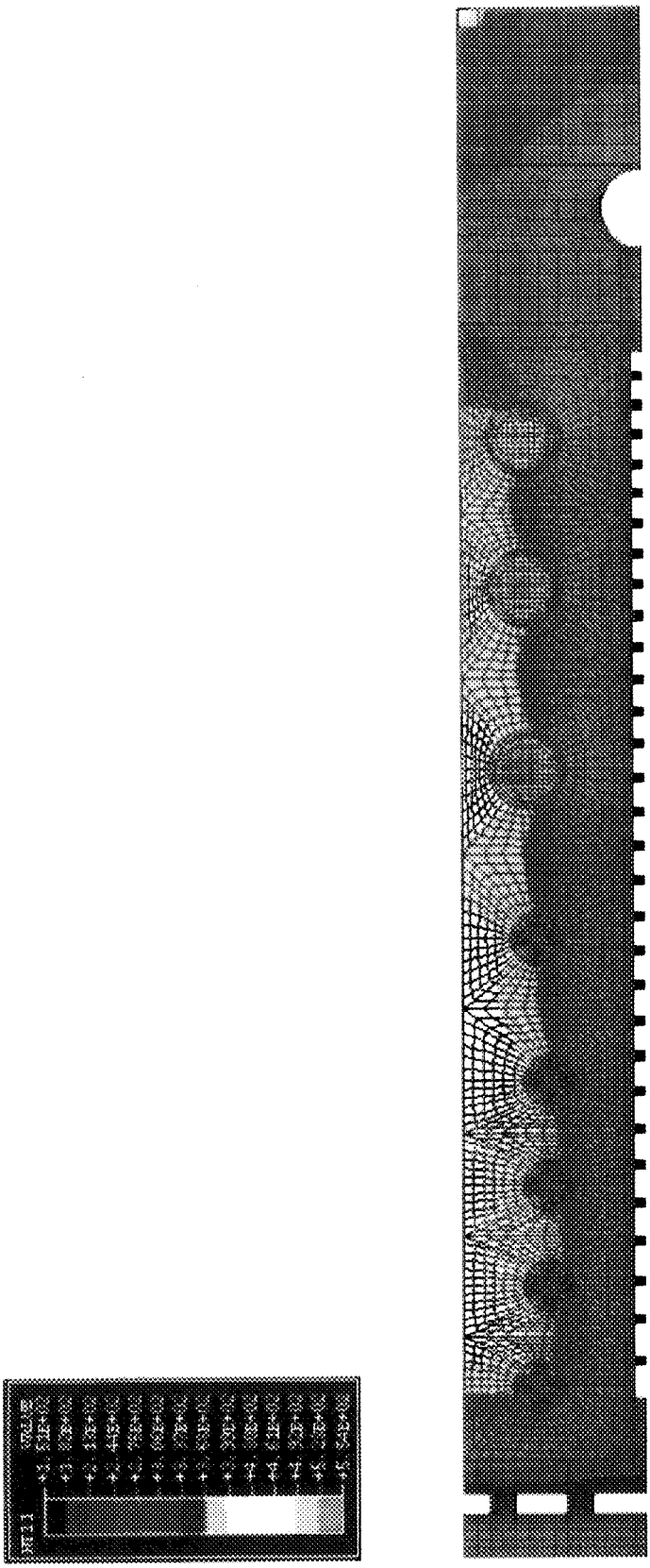

Fig. 5.5 Analyzed result of ITER #19 bleeding blanket
(Case A-nominal : Temperature distribution)

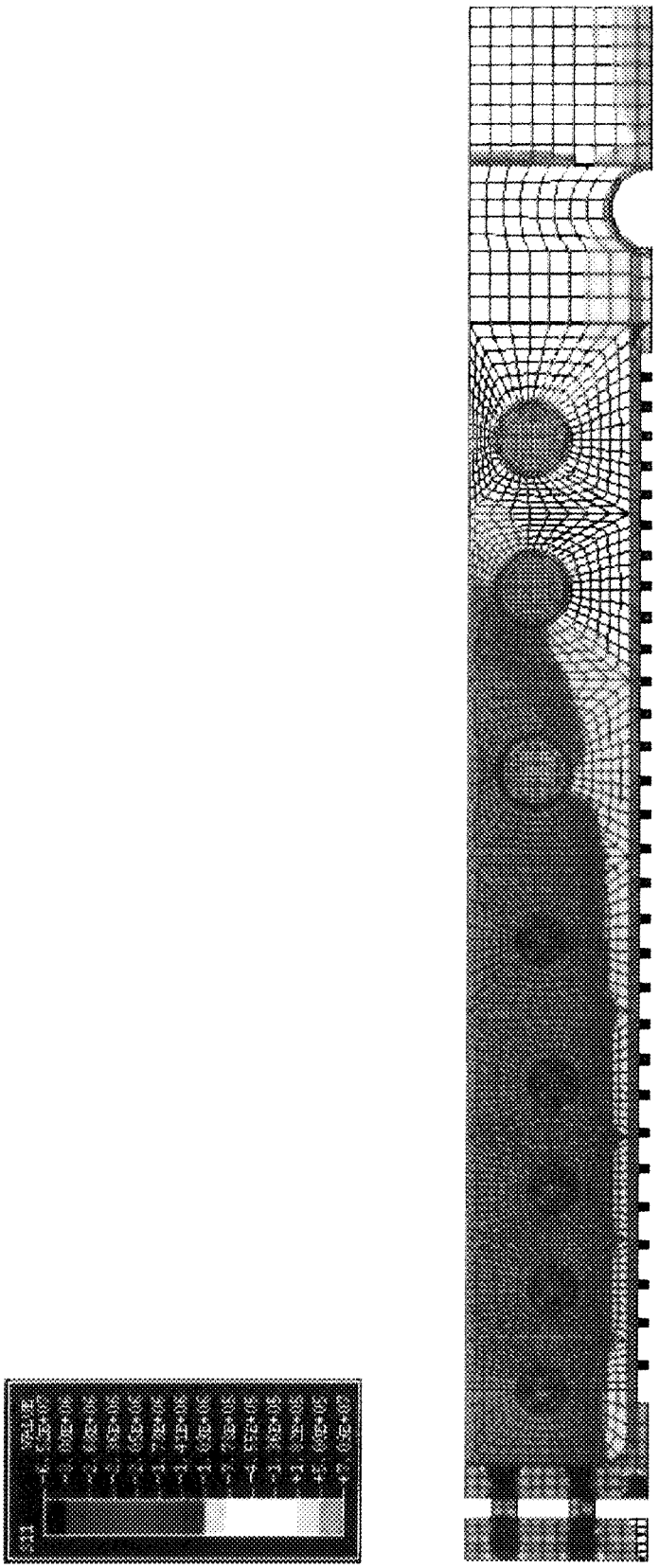

Fig. 5.6 Analyzed result of ITER #19 bleeding blanket
(Case A-nominal : σ -X distribution)

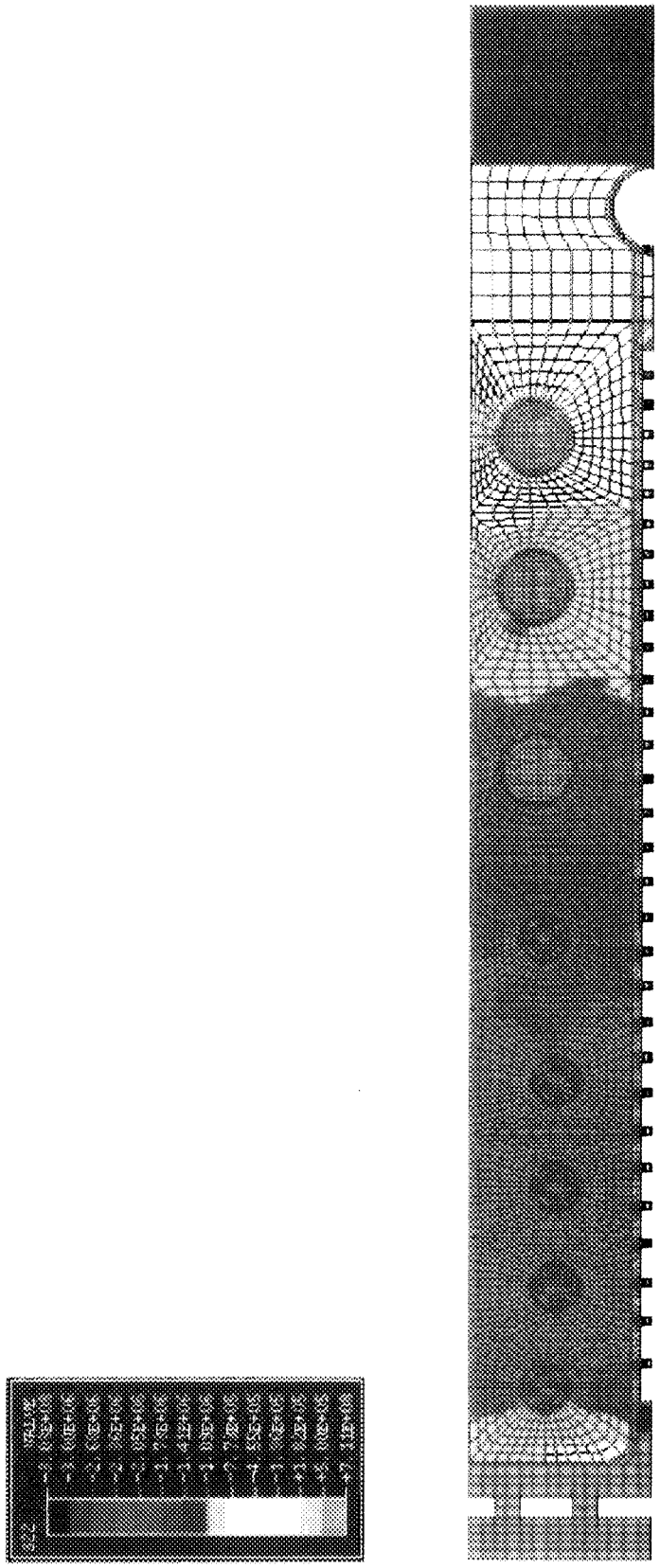

Fig. 5.7 Analyzed result of ITER #19 bleeding blanket
(Case A-nominal : σ -Y distribution)

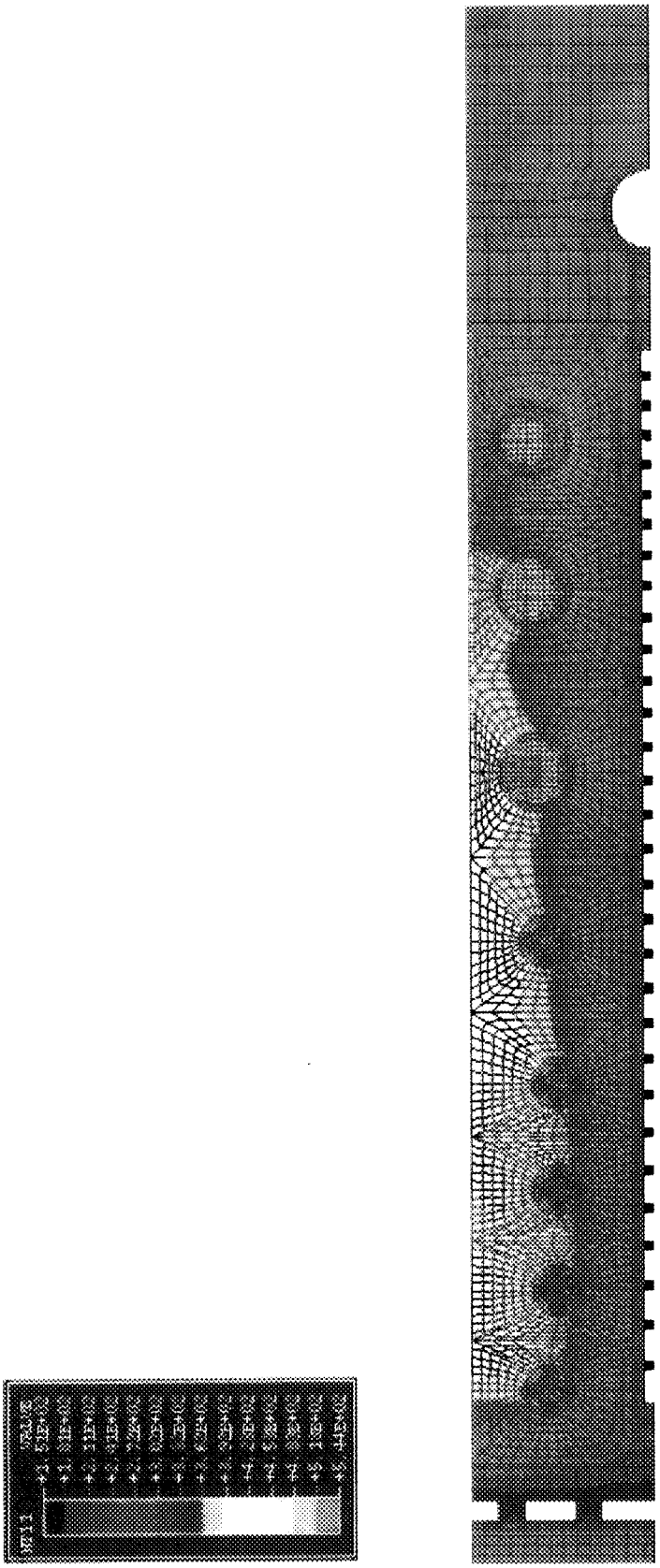

Fig. 5.8 Analyzed result of ITER #19 bleeding blanket
(Case B- λ =13.43W/mK : Temperature distribution)

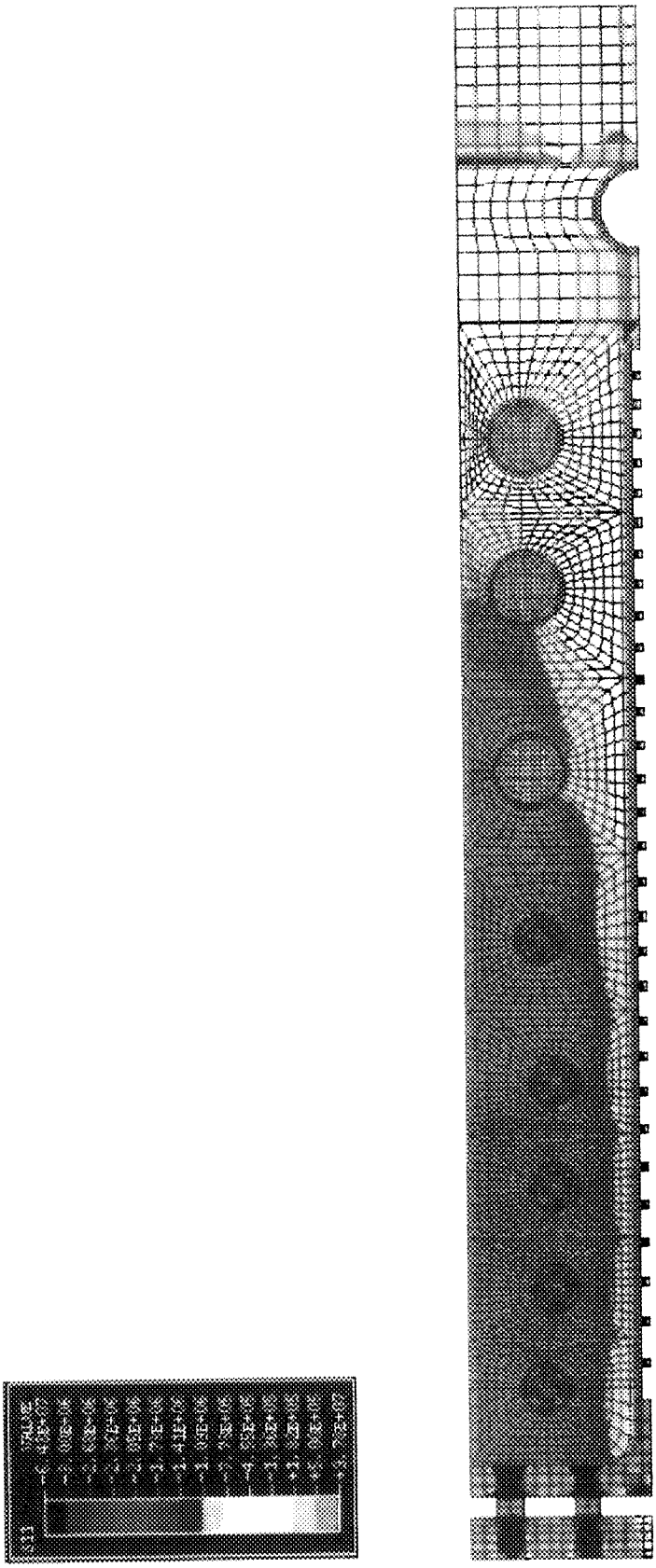

Fig. 5.10 Analyzed result of ITER #19 bleeding blanket
(Case B- λ =13.43W/mK : σ -Y distribution)

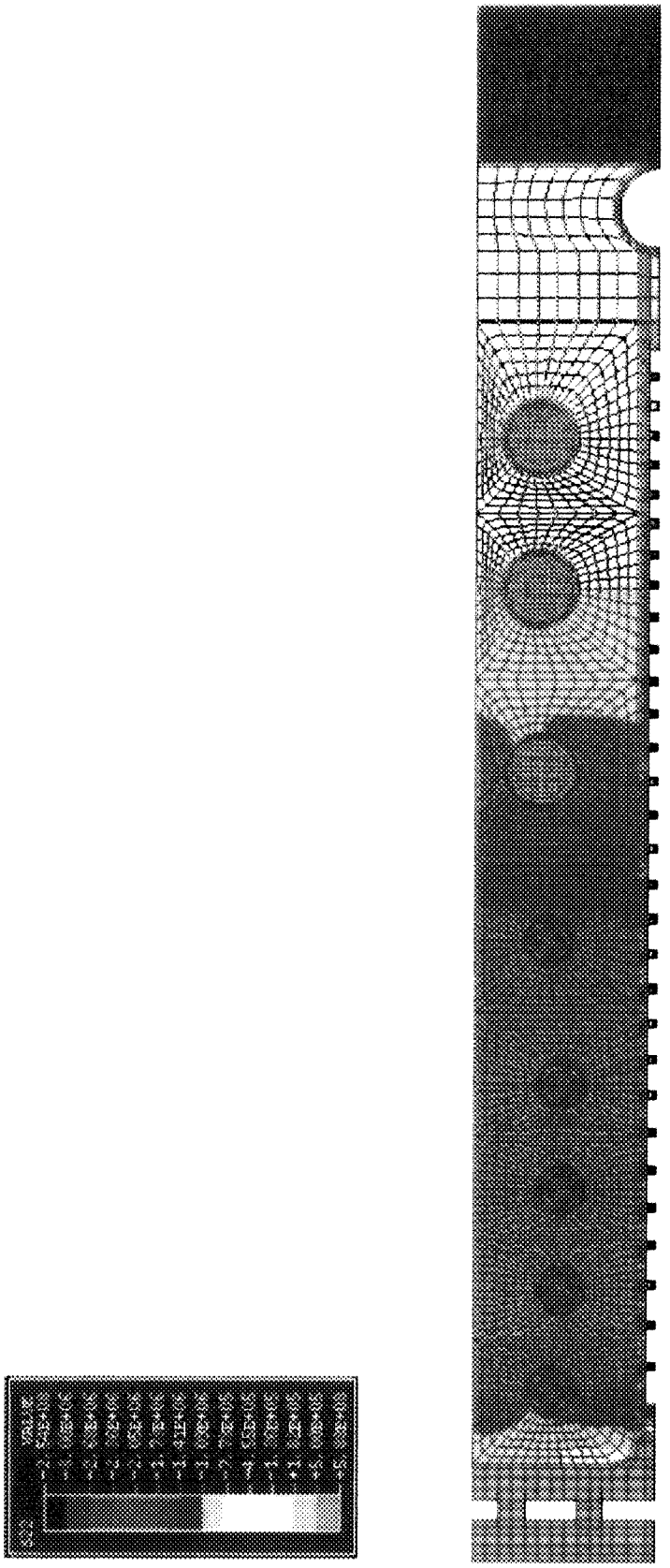

Fig. 5.9 Analyzed result of ITER #19 bleeding blanket
(Case B- λ =13.43W/mK : σ -X distribution)

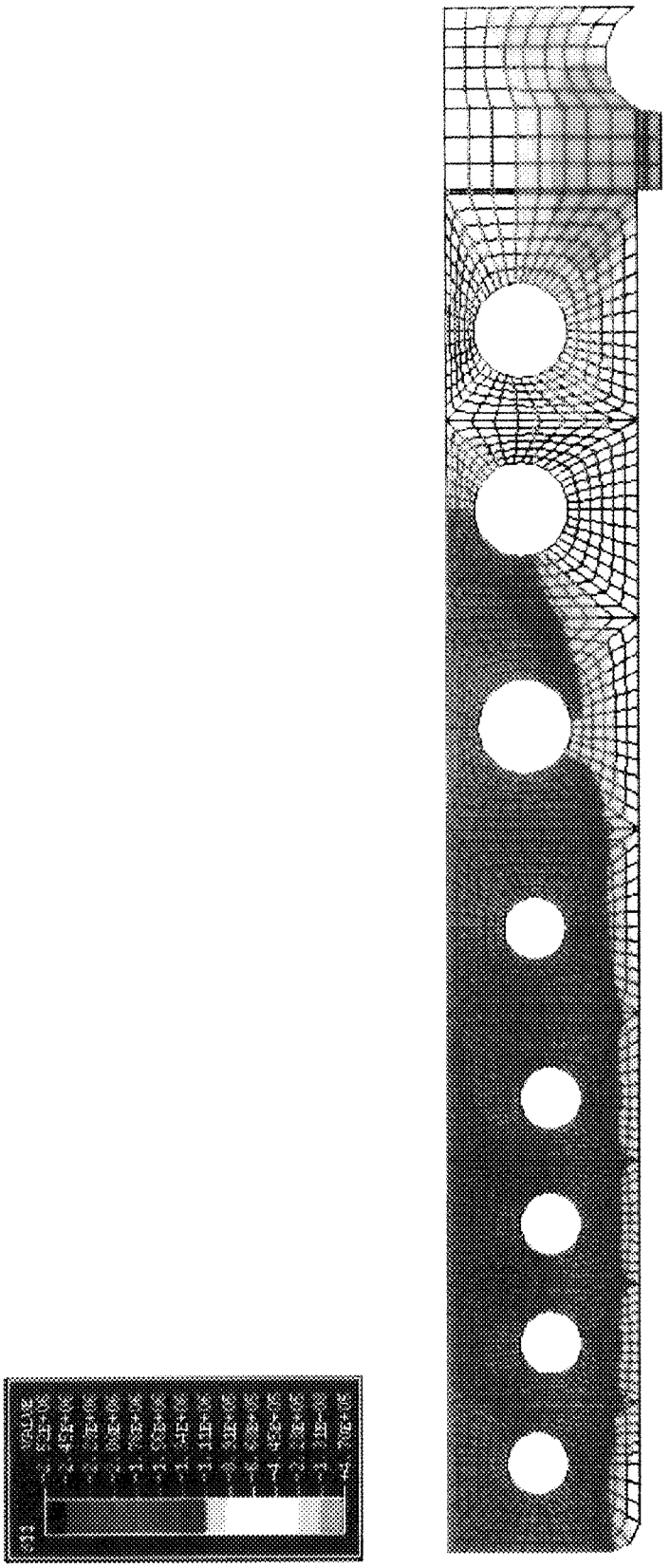

Fig. 5.11 Analyzed result of ITER #19 bleeding blanket
(Case A-nominal : σ -X distribution in Be pebble bed)

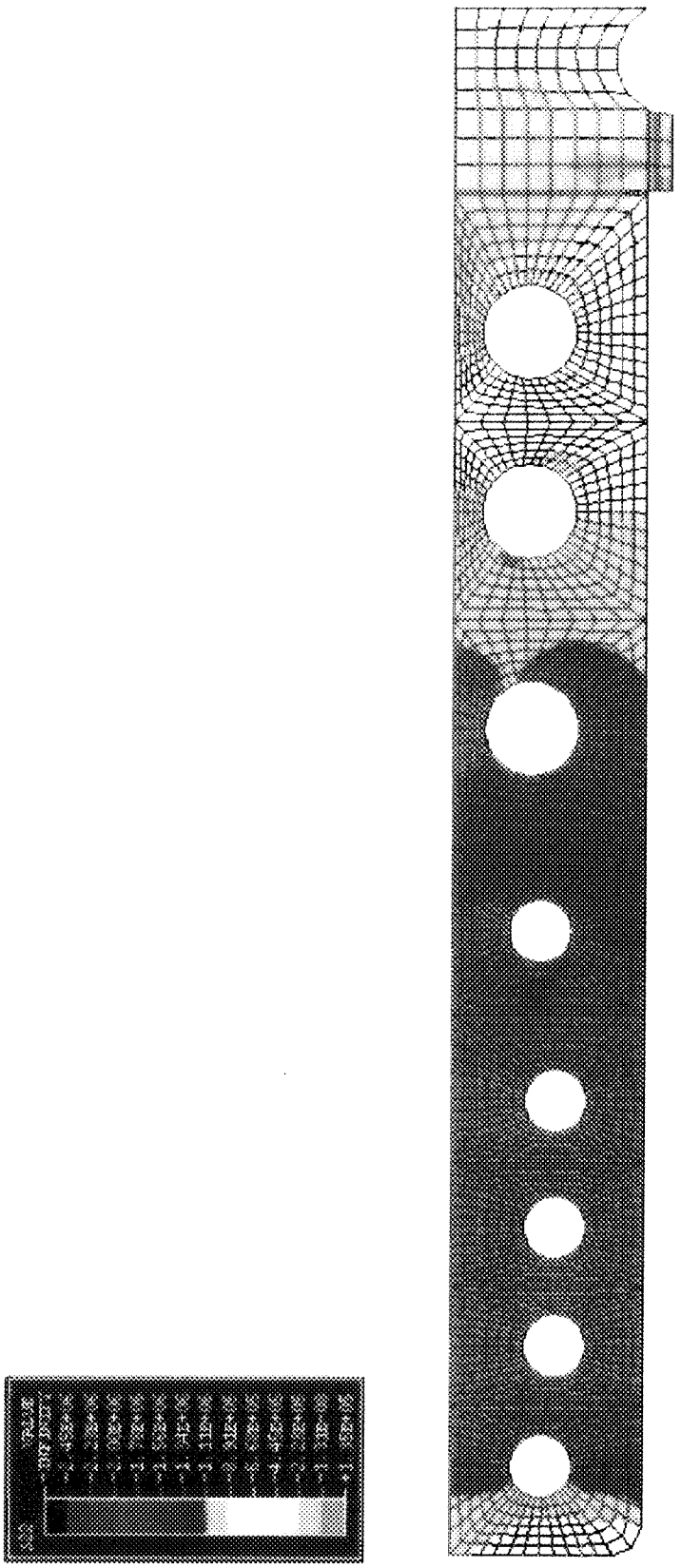

Fig. 5.12 Analyzed result of ITER #19 bleeding blanket
(Case A-nominal : σ -Y distribution in Be pebble bed)

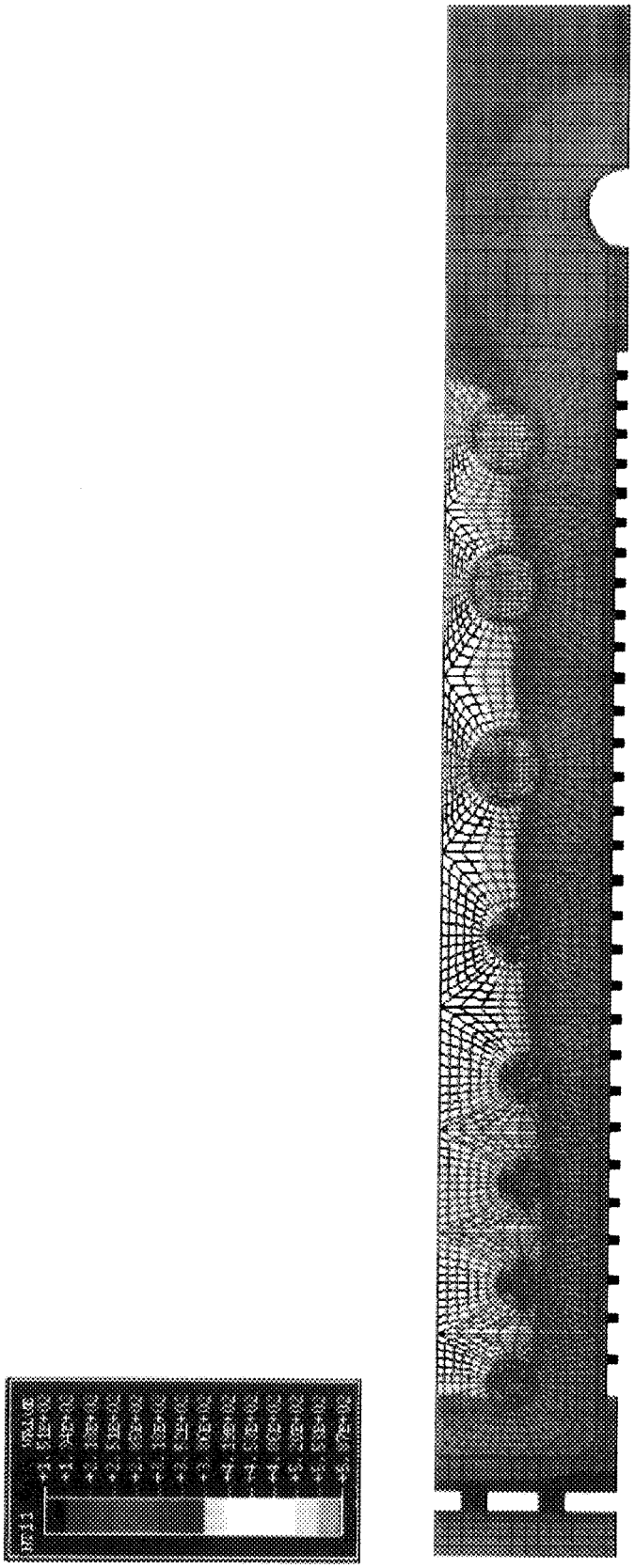

Fig. 5.13 Analyzed result of ITER #19 bleeding blanket
(Case B- λ =-20% : Temperature distribution)

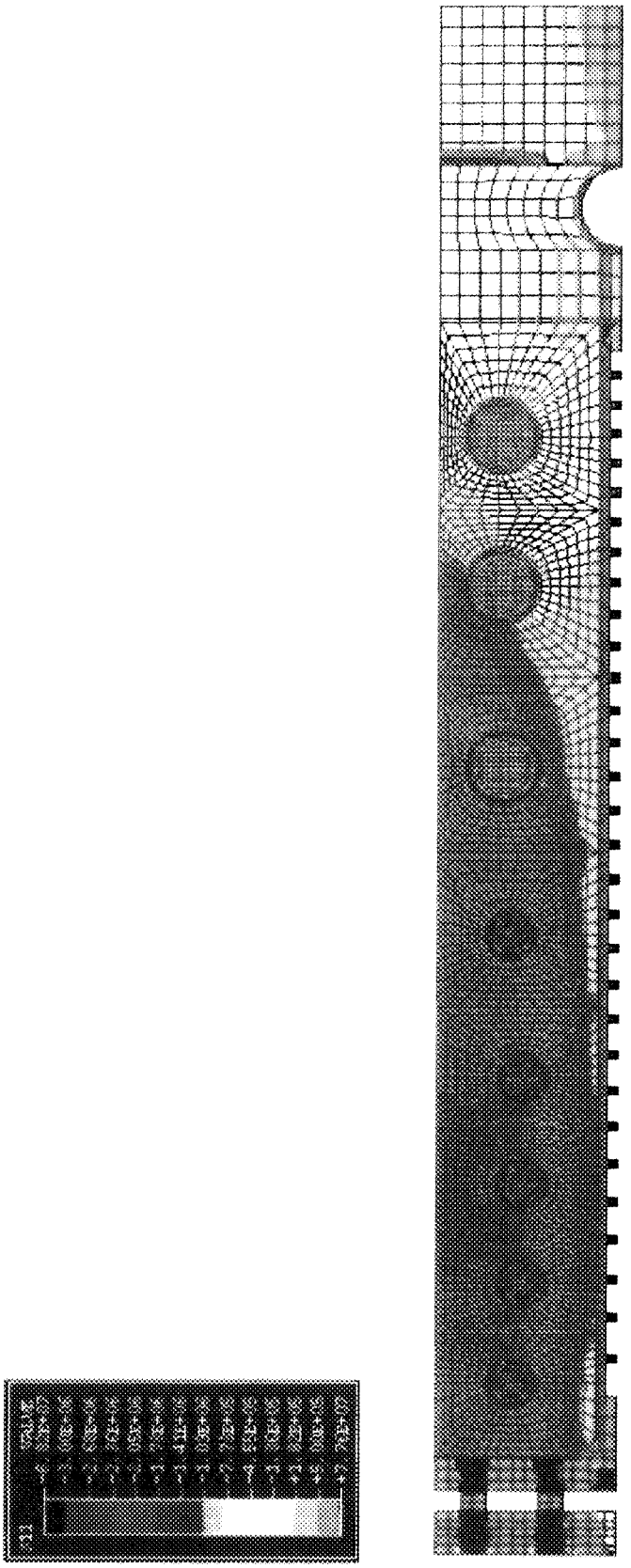

Fig. 5.14 Analyzed result of ITER #19 bleeding blanket
(Case B- λ =-20%: σ -X distribution)

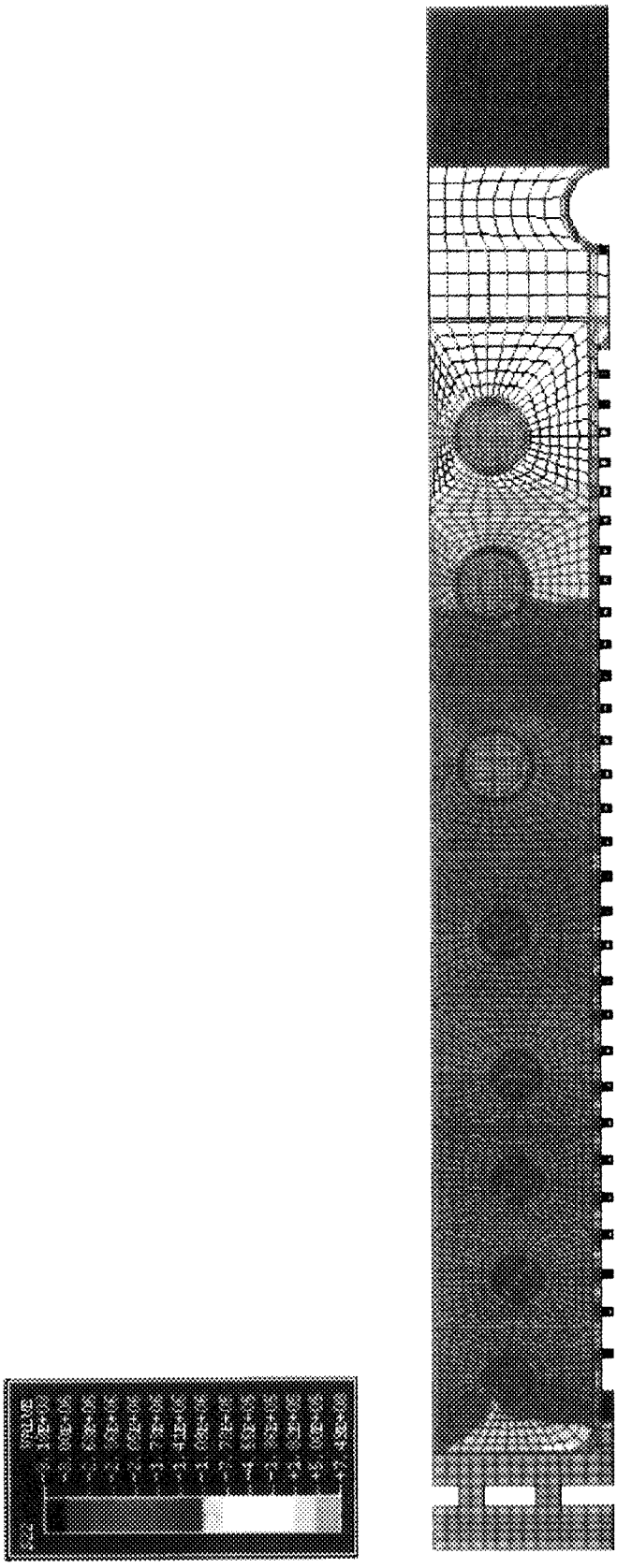

Fig. 5.15 Analyzed result of ITER #19 bleeding blanket
(Case B- λ =-20%: σ -Y distribution)

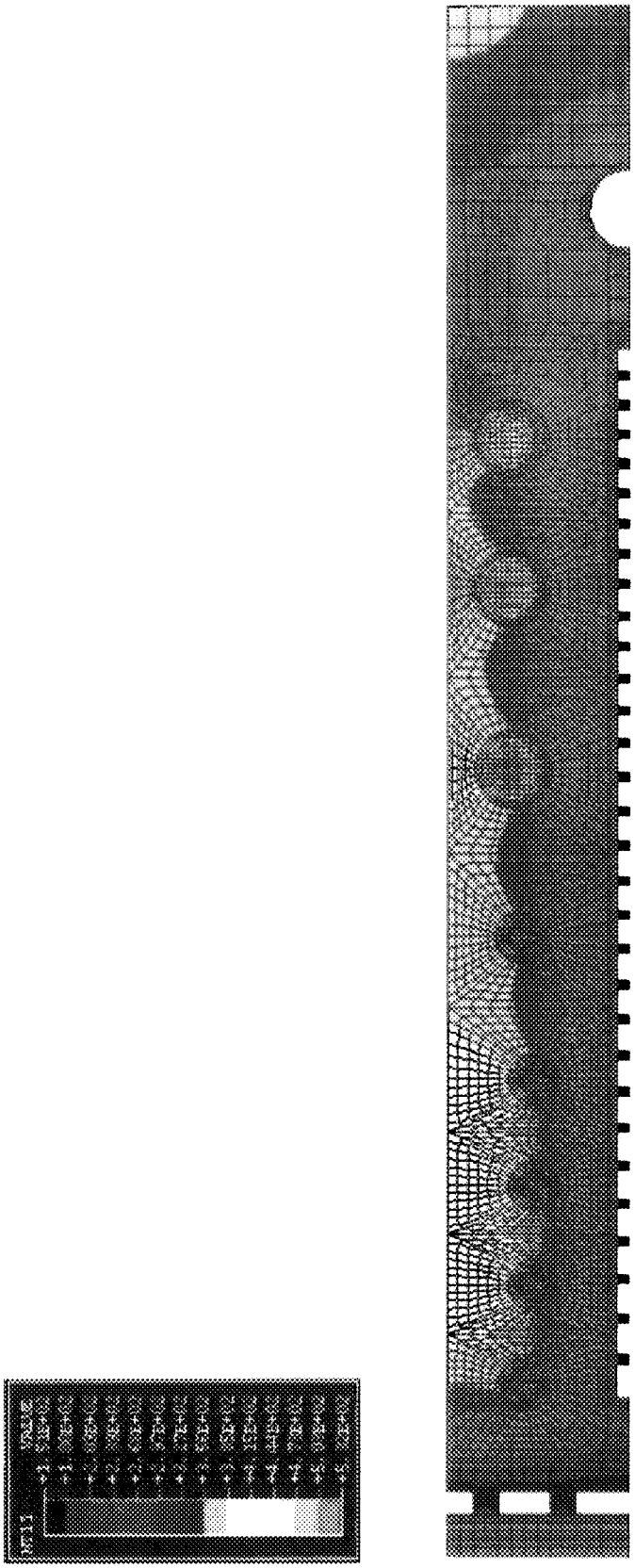

Fig. 5.16 Analyzed result of ITER #19 bleeding blanket
(Case B- λ =+20% : Temperature distribution)

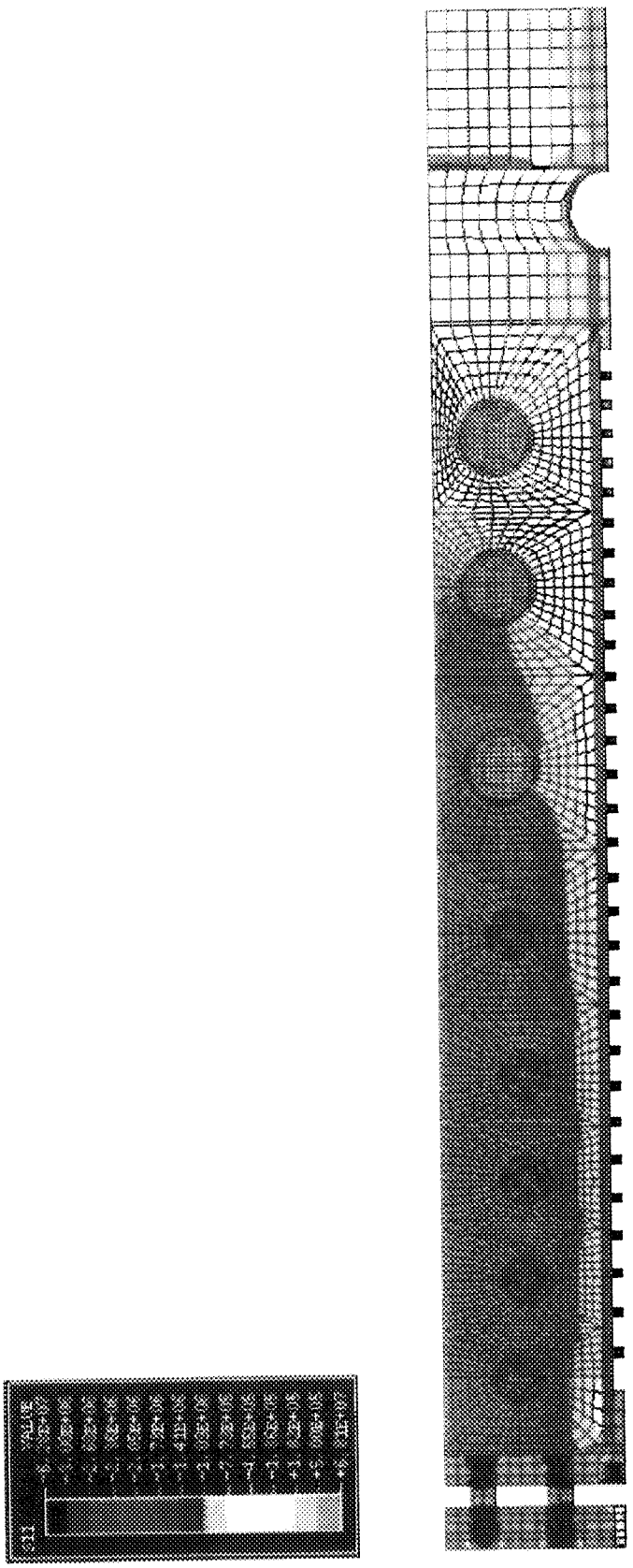

Fig. 5.17 Analyzed result of ITER #19 bleeding blanket
(Case B- λ =+20%: σ -X distribution)

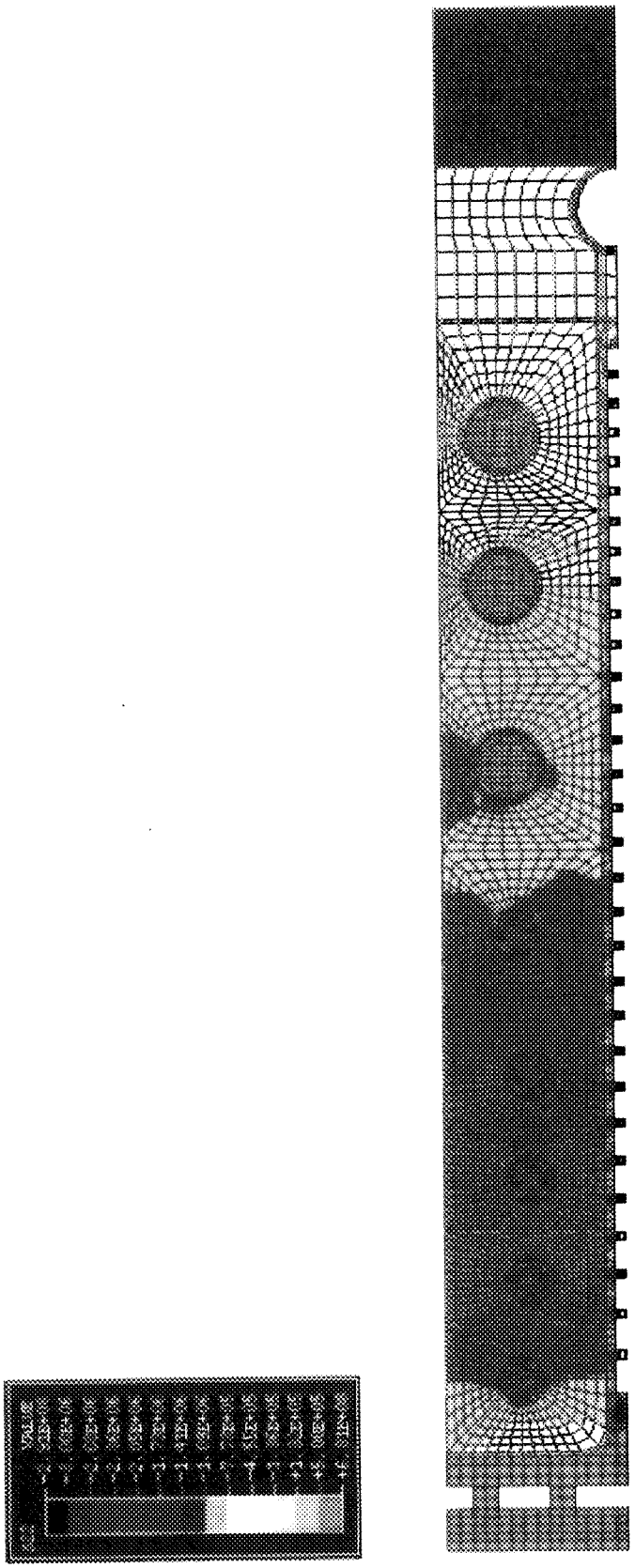

Fig. 5.18 Analyzed result of ITER #19 bleeding blanket
(Case B- λ =+20%: σ -Y distribution)

6. Summary

Thermo-mechanical analysis of #19 ITER breeding blanket module has been conducted taking into account spatially varying thermal conductivity and heat transfer coefficient in Be pebble bed depending on the stresses due to the differential thermal expansion of the blanket.

The modified DRUCKER-PRAGER/Cap plasticity model of ABAQUS code is used because it can deal with such mechanical features of pebble bed as shear failure flow and plastic consolidation. The capability of the model is studied and proved through analysis of the uni-axial compressive experiment.

The thermal conductivity - stress correlation and heat transfer coefficient - stress correlation for Be pebble beds are obtained based on the experimental results and additional thermo-mechanical analysis.

The COUPLED TEMPERATURE-DISPLACEMENT procedure of ABAQUS code is used so that thermal conductivity is automatically calculated in each calculation point depending on the stress.

Thermo-mechanical analysis of the ITER breeding blanket module has been performed for four conditions: case A; nominal case, case B; constant thermal conductivity (13.43 W/mK), case C; thermal conductivity = -20% of nominal case ,and case D; thermal conductivity = +20% of nominal case.

- In the nominal case the temperature of breeding material (Li_2ZrO_3) ranges from 317℃ to 554℃. The maximum temperature of Be pebble bed is 446℃.
- The breeder temperatures in 8^{th} tube and the shielding plate in case A are higher than those for case B because of lower thermal conductivity caused by lower compressive stresses. It might be concluded that the spatially constant thermal conductivity estimated by FZK is fairly good as a whole for ITER type breeding blanket.
- Current design of ITER breeding blanket is evaluated to permit $\pm 20\%$ change in thermal conductivity of Be pebble bed.

From the analysis for the uni-axial compressive and the heat transfer experiment, it is confirmed that the analysis method and model taken here qualitatively represent well the pebble bed behaviors observed in the experiment. Preliminarily analysis on the ITER breeding blanket shows the present design will satisfy the currently specified material temperature limits. For more detail quantitative estimates of the blanket performance, further investigation on mechanical properties of pebble beds by experiment and the improvement of the analysis model and the calculation code are required.

Acknowledgment

The authors wish to acknowledge Drs. S. Matsuda, Y. Seki, T. Nagashima, T. Tsunematsu and M. Seki for their support. They are also grateful to Dr. Takatsu and Dr. Ohara for his continuous encouragement. This work has been performed in the framework of ITER Design Task. Then the authors are also grateful to Drs. Y. Gohar, K. Mohri and K. Ioki of the ITER Joint Central Team for valuable information on breeding blanket configuration and constructive discussions.

Reference

[1] Y. Gohar, Personal Communication, Breeding Blanket group of ITER Joint Central Team, 1997.

[2] M. Ferrari et al., ITER Reference Breeding Blanket Design, 20th Symp. Fusion Technol. Sept., 1998, Marseille, France..

[3] J. Feda, Mechanics of Particle Materials The Principles, Elsevier Scientific Publishing Company, 1982.

[4] Alice Y.Ying et al., Mechanical Behavior and Design Database of Packed Beds for Blanket Designs, ISFNT-4, Tokyo, Japan, April(1997)

[5] M. Dalle Donne et al., Measurement of the Thermal conductivity and Heat Transfer Coefficient of a Binary Bed of beryllium Pebbles, Proc., 3rd IEA International Work shop on Beryllium Technology for Fusion, Mito, Japan, Oct., 1997.

[6] ABAQUS THEORY MANUAL and ABAQUS/Standard User's Manual, Hibbitt, Karlsson & Sornsen, INC

[7] F. Tehranian and M. Abdou, Experimental Study of the Effect of External Pressure on Particle Bed Effective Thermal Properties, Fus. Technol., 27(1995)

[8] K. Walton, "The effective Elastic Modulus of a Random Packing of Sphere", J. Mech. Phis. Solids, Vol. 35, No. 2, pp. 213-226, 1987

[9] A. L. Endres, The Effect of Contact Generation on the Elastic Properties of a Granular Medium, Trans. ASME, 57(1990)330-336

[10] E. U. Schlunder and R. Bauer, Inter. Chem. Eng. 18(1978),181

[11] ITER Material Properties Handbook, Oct. 1997.

[12] M. C. Billone, et al., ITER Solid Breeder Blanket materials Database, ANL/FPP/TM-263, Nov., 1993.

[13] A. C. Paine, Elastic Properties of Granular Materials, Univ. of Bath, 1998.

Appendix A

Calculations of Young's modulus of pebble bed

An analytic method for estimating Young's modulus of a random packed single size pebble bed is reported by K.Walton [8]. This method is used here despite of its applicability for only single size pebble bed. It is because a newly proposed method improved to deal with binary pebble beds [13] cannot be used here due to lack of available data on binary pebble bed at present (e.g. number of contact points between pebbles). In the method of K.Walton, Young's modulus of pebble bed is calculated as a proportional coefficient between stress and strain averaged over pebble bed. The stress is computed with a given strain by an elastic theory on contact of pebbles. The relation between the strain and the stress is analyzed in incremental form since young's modulus generally depends on a strain in pebble bed.

Young's modulus is given by the next equation for uniaxial strain and no friction between pebbles.

$$\alpha = \frac{\phi n e^{1/2}}{32\pi^2 B}$$

C_{11}^* (Young's modulus) = 3α

Φ : 0.808 (packing factor)
n : 6.4 (number of average contacts points per one pebble)
e : 0.001 (strain)

$$B = \frac{1}{4\pi}\left(\frac{1}{\mu} + \frac{1}{\lambda + \mu}\right)$$

λ: 2.14×10^{10} [Pa] (Lame's constants)
μ: 1.31×10^{11} [Pa] (Lame's constants)

C_{11}^*: 1.38×10^{9} [Pa] (Young's modulus for pebble bed)

(Above variables were used to calculate Young's modulus of Be pebble bed in Table 5.2)

Appendix B Thermal and mechanical property

SS316

Temperature (°C)	Thermal Conductivity (W/m-K)	Thermal Expansion (1/K)	Young's Modulus (Pa)	Poisson's Ratio
20	13.94	1.59E-05	1.92E+11	0.3
50	14.37	1.61E-05	1.90E+11	0.3
100	15.08	1.64E-05	1.86E+11	0.3
150	15.8	1.67E-05	1.82E+11	0.3
200	16.52	1.70E-05	1.78E+11	0.3
250	17.24	1.72E-05	1.74E+11	0.3
300	17.95	1.75E-05	1.70E+11	0.3
350	18.67	1.77E-05	1.66E+11	0.3
400	19.39	1.79E-05	1.61E+11	0.3
450	20.1	1.81E-05	1.57E+11	0.3
500	20.82	1.83E-05	1.53E+11	0.3
550	21.54	1.85E-05	1.49E+11	0.3
600	22.26	1.87E-05	1.45E+11	0.3
650	22.97	1.89E-05	1.41E+11	0.3
700	23.69	1.91E-05	1.37E+11	0.3
800	25.12	1.93E-05	1.29E+11	0.3

Be

Temperature (°C)	Thermal Conductivity (W/m-K)	Thermal Expansion (1/K)	Young's Modulus (Pa)	Poisson's Ratio
20	184.51	1.13E-05	3.08E+11	0.071
50	176.95	1.19E-05	3.06E+11	0.07
100	165.3	1.29E-05	3.04E+11	0.069
150	154.77	1.38E-05	3.03E+11	0.068
200	145.29	1.47E-05	3.02E+11	0.067
250	136.77	1.55E-05	3.00E+11	0.065
300	129.14	1.63E-05	2.98E+11	0.064
350	122.33	1.70E-05	2.94E+11	0.063
400	116.26	1.77E-05	2.88E+11	0.062
450	110.86	1.83E-05	2.79E+11	0.06
500	106.05	1.88E-05	2.67E+11	0.059
550	101.75	1.94E-05	2.51E+11	0.058
600	97.89	1.99E-05	2.32E+11	0.057
650	94.39	2.03E-05	2.07E+11	0.055
700	91.17	2.07E-05	1.76E+11	0.054
800	85.3	2.15E-05	9.70E+10	0.052

This is a blank page.

国際単位系 (SI) と換算表

表 1　SI基本単位および補助単位

量	名称	記号
長さ	メートル	m
質量	キログラム	kg
時間	秒	s
電流	アンペア	A
熱力学温度	ケルビン	K
物質量	モル	mol
光度	カンデラ	cd
平面角	ラジアン	rad
立体角	ステラジアン	sr

表 2　SIと併用される単位

名称	記号
分，時，日	min，h，d
度，分，秒	°，′，″
リットル	l，L
トン	t
電子ボルト	eV
原子質量単位	u

1 eV = 1.60218 × 10^{-19} J

1 u = 1.66054 × 10^{-27} kg

表 5　SI接頭語

倍数	接頭語	記号
10^{18}	エクサ	E
10^{15}	ペタ	P
10^{12}	テラ	T
10^{9}	ギガ	G
10^{6}	メガ	M
10^{3}	キロ	k
10^{2}	ヘクト	h
10^{1}	デカ	da
10^{-1}	デシ	d
10^{-2}	センチ	c
10^{-3}	ミリ	m
10^{-6}	マイクロ	μ
10^{-9}	ナノ	n
10^{-12}	ピコ	p
10^{-15}	フェムト	f
10^{-18}	アト	a

表 3　固有の名称をもつSI組立単位

量	名称	記号	他のSI単位による表現
周波数	ヘルツ	Hz	s^{-1}
力	ニュートン	N	$m \cdot kg/s^2$
圧力，応力	パスカル	Pa	N/m^2
エネルギー，仕事，熱量	ジュール	J	N·m
工率，放射束	ワット	W	J/s
電気量，電荷	クーロン	C	A·s
電位，電圧，起電力	ボルト	V	W/A
静電容量	ファラド	F	C/V
電気抵抗	オーム	Ω	V/A
コンダクタンス	ジーメンス	S	A/V
磁束	ウェーバ	Wb	V·s
磁束密度	テスラ	T	Wb/m^2
インダクタンス	ヘンリー	H	Wb/A
セルシウス温度	セルシウス度	℃	
光束	ルーメン	lm	cd·sr
照度	ルクス	lx	lm/m^2
放射能	ベクレル	Bq	s^{-1}
吸収線量	グレイ	Gy	J/kg
線量当量	シーベルト	Sv	J/kg

表 4　SIと共に暫定的に維持される単位

名称	記号
オングストローム	Å
バーン	b
バール	bar
ガル	Gal
キュリー	Ci
レントゲン	R
ラド	rad
レム	rem

1 Å = 0.1 nm = 10^{-10} m

1 b = 100 fm^2 = 10^{-28} m^2

1 bar = 0.1 MPa = 10^5 Pa

1 Gal = 1 cm/s^2 = 10^{-2} m/s^2

1 Ci = 3.7 × 10^{10} Bq

1 R = 2.58 × 10^{-4} C/kg

1 rad = 1 cGy = 10^{-2} Gy

1 rem = 1 cSv = 10^{-2} Sv

（注）

1. 表1～5は「国際単位系」第5版，国際度量衡局 1985年刊行による。ただし，1 eVおよび1 uの値はCODATAの1986年推奨値によった。
2. 表4には海里，ノット，アール，ヘクタールも含まれているが日常の単位なのでここでは省略した。
3. barは，JISでは流体の圧力を表わす場合に限り表2のカテゴリーに分類されている。
4. EC閣僚理事会指令ではbar，barnおよび「血圧の単位」mmHgを表2のカテゴリーに入れている。

換　算　表

力	N(=10^5 dyn)	kgf	lbf
	1	0.101972	0.224809
	9.80665	1	2.20462
	4.44822	0.453592	1

粘度　1 Pa·s(N·s/m^2) = 10 P(ポアズ)(g/(cm·s))

動粘度　1 m^2/s = 10^4 St(ストークス)(cm^2/s)

圧力	MPa(=10 bar)	kgf/cm^2	atm	mmHg(Torr)	lbf/in^2(psi)
	1	10.1972	9.86923	7.50062 × 10^3	145.038
	0.0980665	1	0.967841	735.559	14.2233
	0.101325	1.03323	1	760	14.6959
	1.33322 × 10^{-4}	1.35951 × 10^{-3}	1.31579 × 10^{-3}	1	1.93368 × 10^{-2}
	6.89476 × 10^{-3}	7.03070 × 10^{-2}	6.80460 × 10^{-2}	51.7149	1

エネルギー・仕事・熱量	J(=10^7 erg)	kgf·m	kW·h	cal(計量法)	Btu	ft·lbf	eV
	1	0.101972	2.77778 × 10^{-7}	0.238889	9.47813 × 10^{-4}	0.737562	6.24150 × 10^{18}
	9.80665	1	2.72407 × 10^{-6}	2.34270	9.29487 × 10^{-3}	7.23301	6.12082 × 10^{19}
	3.6 × 10^6	3.67098 × 10^5	1	8.59999 × 10^5	3412.13	2.65522 × 10^6	2.24694 × 10^{25}
	4.18605	0.426858	1.16279 × 10^{-6}	1	3.96759 × 10^{-3}	3.08747	2.61272 × 10^{19}
	1055.06	107.586	2.93072 × 10^{-4}	252.042	1	778.172	6.58515 × 10^{21}
	1.35582	0.138255	3.76616 × 10^{-7}	0.323890	1.28506 × 10^{-3}	1	8.46233 × 10^{18}
	1.60218 × 10^{-19}	1.63377 × 10^{-20}	4.45050 × 10^{-26}	3.82743 × 10^{-20}	1.51857 × 10^{-22}	1.18171 × 10^{-19}	1

1 cal = 4.18605 J（計量法）

= 4.184 J　（熱化学）

= 4.1855 J　（15 °C）

= 4.1868 J（国際蒸気表）

仕事率　1 PS（仏馬力）

= 75 kgf·m/s

= 735.499 W

放射能	Bq	Ci
	1	2.70270 × 10^{-11}
	3.7 × 10^{10}	1

吸収線量	Gy	rad
	1	100
	0.01	1

照射線量	C/kg	R
	1	3876
	2.58 × 10^{-4}	1

線量当量	Sv	rem
	1	100
	0.01	1

（86年12月26日現在）

PRELIMINARY THERMO-MECHANICAL ANALYSIS OF ITER BREEDING BLANKET